Hindawi
Mathematical Problems in Engineering
Volume 2020, Article ID 4580467, 23 pages
https://doi.org/10.1155/2020/4580467

Research Article

Sound Transmission in the First Nonlinear Model of Middle Ear with an Active Implant

Rafal Rusinek

Lublin University of Technology, Nadbystrzycka 36, 20-618 Lublin, Poland

Correspondence should be addressed to Rafal Rusinek; r.rusinek@pollub.pl

Received 12 June 2019; Revised 6 September 2019; Accepted 16 September 2019; Published 3 January 2020

Academic Editor: Krzysztof Puszynski

This paper shows an influence of a transducer of a middle ear implant on ear dynamics on the basis of the multi-degree-of-freedom biomechanical system. Results of numerical simulations of an ear model with implant are compared with those of the healthy middle ear. Two variants of damping are analysed. The first one typical for a normal healthy middle ear structure and the second one describes pathological properties of the human ear. Moreover, the behaviour of the transducer under various external excitations is investigated. For some set of parameters, the middle ear with the implant behaves regularly but sometimes even chaotically in case of strong excitation.

1. Introduction

The human ear is composed of three parts: the outer, the middle, and the internal (inner) ear. Sound, approaching to the ear, is transmitted from the outer to the inner part through the middle ear. The human middle ear (HME) is a small biomechanical system, which consists of the tympanic membrane, three ossicles (i.e., the malleus, the incus, and the stapes), as well as ligaments and tendons that fix ossicles to each other and to the temporal bone as well. Sound approaching to the outer ear in the form of acoustic pressure is transformed into mechanical vibrations in the middle ear and next to an electrical signal in the inner ear. Since the middle ear is the smallest and one of the most complicated biomechanical structures in the human body, its treatment is especially demanding and difficult. Of course, it depends on a type of hearing loss. Generally, two types of hearing loss are defined: conductive and sensorineural. The former is usually treated by means of prostheses of different types that are passive elements connecting damaged or missing ossicles. The latter can be healed by a cochlear implant in case of profound hearing loss, but most mild to moderate sensorineural hearing losses are still compensated by traditional hearing aids. However, conventional hearing aids have several inherent disadvantages, such as sound distortion, limited amplification, noise and ringing, discomfort, and cosmetic appearance [1]. Therefore, in recent years, new solutions of active middle ear implants have been used in medical practice as an alternative to the conventional treatment method. These devices are known as implantable middle ear hearing devices (IMEHDs) and can be used in case of sensorineural hearing loss and sometimes in different structural configurations also in conductive hearing loss. A typical IMEHD consists of three parts (Figure 1): the microphone, the signal processing, and the vibrating output transducer called as the floating mass transducer (FMT). Numerous procedures are currently used in clinical practice to implant the hearing device. An otolaryngologist must find the best position of a vibrating transducer and the method to fix it to the ossicular chain by means of a coupler (clip). The FMT is the main part of the IMEHD which provides a direct mechanical stimulation to the human ear [1, 2]. The ossicular chain is the component that the transducer commonly stimulates, and then the vibration is transmitted into the cochlea through the oval window. However, coupling the transducer to the ossicular chain is difficult in case of patients with middle ear disease, such as ossicular lesion. To solve this problem, an alternative way of coupling the

transducer to the cochlea by driving the round window (RW), called RW stimulation, is developed [1]. The RW simulation can improve various conductive and mixed hearing losses, even though this method needs static preload to the RW.

Clinical studies on this IMEHD's application have been reported by several authors [3, 4, 5], but the human middle ear with the IMEHD is explored mainly experimentally or by means of FEM. Undoubtedly, there is a lack of a nonlinear mechanical lumped mass model that can explain the human middle ear and the implant behaviour. To the best of our knowledge, only one paper with the lumped mass model has been published [6]. The authors show a simple linear model without deep investigation; therefore, here a sensitivity analysis of the implant parameters and external excitation on the middle ear is the main goal of the study.

This paper is organized as follows: Section 2 presents a three-degree-of-freedom (3dof) model of the normal middle ear (NME) and a 5dof model of the human middle ear with an implant (implanted middle ear, IME), which consists of the NME and the IMEHD. In Section 3, a natural frequency analysis of the undamped linear and the nonlinear model of the NME is presented. Next, a simplified linear model of the IME and finally a nonlinear one are investigated to compare the results with outcomes obtained in the case of the NME. Finally, discussion of results and conclusions are presented in Section 5.

2. Model of the Human Middle Ear

Most often, the human middle ear is modelled in the literature by means of a finite element method (FEM) which is useful in practical applications but weaker in achieving knowledge and developing a new theory of the middle ear. Therefore, various lumped mass models are developed to overcome these limitations starting from three [7], four [8], and sometimes even six [9] degrees of freedom (dof). However, these models are only linear that cannot reflect the middle ear complex behaviour.

Here, the 3dof nonlinear model of the normal (healthy, NME) middle ear, called shortly as a normal middle ear (NME), is proposed. Next, the model is extended to the 5dof for the IME. Moreover, in the paper, two sets of parameters are used: the standard parameters that are typical for a healthy ear and the pathological ones where damping coefficients are decreased, but the ossicular chain is still intact (not damaged). Therefore, sensorineural hearing loss is investigated in this paper.

Since the model is a form of real object simplification, several important assumptions are made in the middle ear model. First of all, the model is prepared for low frequencies. Therefore, the hydrodynamics of the inner ear and the vibratory characteristics of the basilar membrane are neglected. Moreover, it is assumed that the middle ear reflex is the same in the normal and the implanted middle ear. It is true in the case of mild and moderate hearing loss. The reflex does not depend on sound frequency.

2.1. Normal Ear. The model of the normal human middle ear (Figure 1) is represented by three lumped masses: the malleus (m_M), the incus (m_I), and the stapes (m_S) that are connected to each other and to the temporal bone by the joints (IMJ and ISJ) and ligaments (AML, PIL, and AL). Damping and stiffness properties of the elements are denoted as c and k, respectively, including the cochlea (c_c and k_c) and the tympanic membrane (c_{TM}, k_{TM}). Notice that the AL has nonlinear stiffness characteristics that are talked over in the next section. In the case of the healthy ear (NME), the malleus and the tympanic membrane are stimulated by an outer signal (sound) represented by $Q\cos\omega t$. However, in the sick ear, sound stimulation should be stronger and placed as close to the cochlea as possible.

2.2. Implanted Middle Ear. In case of any hearing loss, e.g., because of illnesses, the middle ear can be stimulated by the IMEHD. Therefore, the biomechanical system of the normal middle ear (3dof system) is developed here by adding the floating mass transducer of an IMEHD, presented in Figure 1. The FMT is fixed to the incus long process by the clip in which linear damping and stiffness coefficients are labelled by c_{CLIP} and k_{CLIP} while nonlinear stiffness by k_{CLIP3}. The transducer is composed of the floating mass (the magnet, M_m) and the metal case (M_c). The floating mass, suspended with dampers (c_m) and springs (k_m), is moved by an electromagnetic field; as a result, the mass oscillates with the amplitude P and frequency ω. Sometimes, the mass of the tympanic membrane and the cochlea are also analysed, and then the system of the middle ear with an active implant would be 7 degrees of freedom (7dof), but here we focus on the 5dof system. The 7dof system would be better for RW stimulation. Since the incus is excited in our model, the 5dof system is investigated.

The model presented in Figure 1 has three nonlinearities. Cubic stiffness ($\widetilde{\gamma}_3$) for the sake of nonlinear properties of the annular ligament (AL) is reported in [10]. The experimental measurements of AL stiffness taken from [10] are compared with the proposed cubic approximation here in Figure 2(a). The clip which fixes the implant to the middle ear structure is also assumed to be nonlinear ($\widetilde{\gamma}_{24}$). Moreover, the silicon rubber suspension of the magnet (M_m) is described by the 3rd order polynomial ($\widetilde{\gamma}_{45}$ and $\widetilde{\beta}_{45}$) because of nonlinear properties of the silicon rubber reported, e.g., in [11, 12]. In Figure 2(b), the polynomial approximation is confronted with the real experiment results, taken from [12]. Thus, the governing differential equations of IME motion in the dimensional form are as follows:

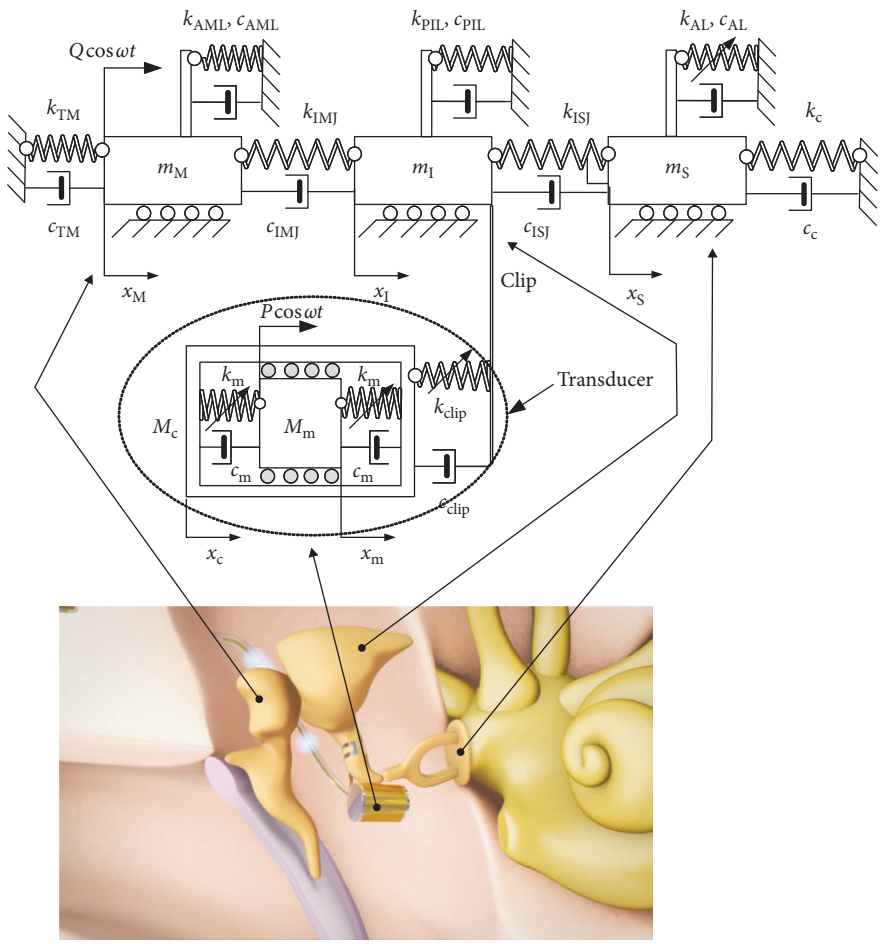

Figure 1: Model of the human middle ear with an active implant.

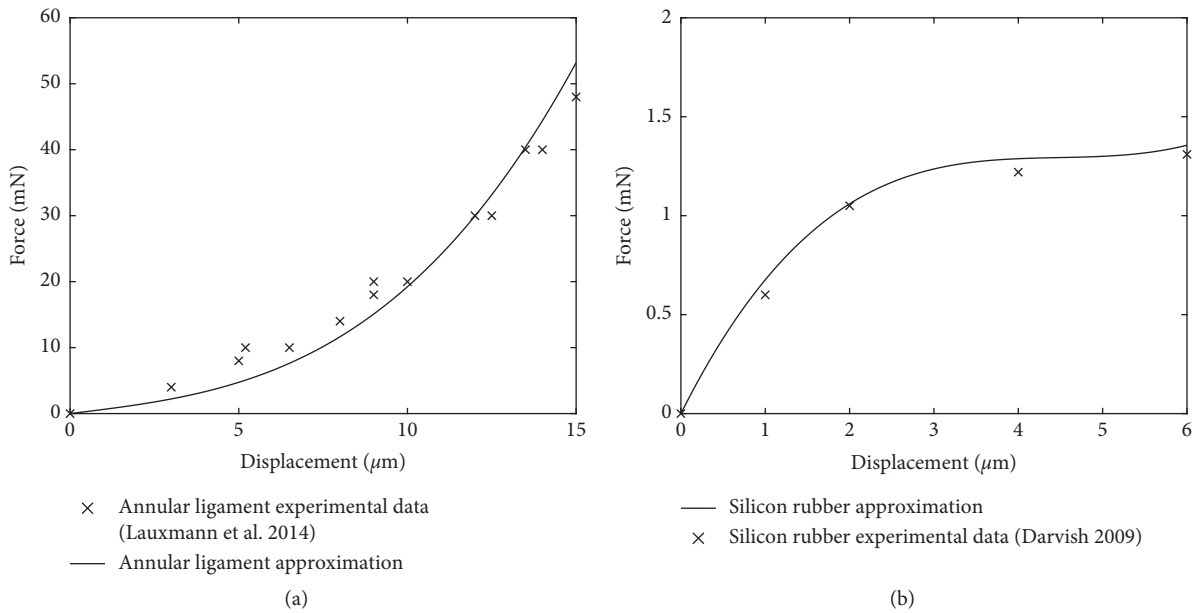

Figure 2: Nonlinear characteristics of the annular ligament (a) and silicon rubber (b).

$$
\begin{aligned}
&\ddot{x}_{\mathrm{M}} m_{\mathrm{M}} + \widetilde{k}_{11} x_{\mathrm{M}} + \widetilde{k}_{12} x_{\mathrm{I}} + \widetilde{c}_{11} \dot{x}_{\mathrm{M}} \\
&+ \widetilde{c}_{12} \dot{x}_{I} = Q \cos(\omega t), \\
&\ddot{x}_{I} m_{\mathrm{I}} + \widetilde{k}_{21} x_{\mathrm{M}} + \widetilde{k}_{22} x_{\mathrm{I}} + \widetilde{k}_{23} x_{\mathrm{S}} + \widetilde{k}_{24} x_{\mathrm{c}} \\
&+ \widetilde{\gamma}_{24} (x_{\mathrm{I}} - x_{\mathrm{c}})^3 + \widetilde{c}_{21} \dot{x}_{\mathrm{M}} + \widetilde{c}_{22} \dot{x}_{\mathrm{I}} + \widetilde{c}_{23} \dot{x}_{\mathrm{S}} + \widetilde{c}_{24} \dot{x}_{\mathrm{c}} = 0, \\
&\ddot{x}_{\mathrm{S}} m_{\mathrm{S}} + \widetilde{k}_{32} x_{\mathrm{I}} + \widetilde{k}_{33} x_{\mathrm{S}} + \widetilde{c}_{32} \dot{x}_{\mathrm{I}} + \widetilde{c}_{33} \dot{x}_{\mathrm{S}} + \widetilde{\gamma}_{3} x_{\mathrm{S}}^3 = 0, \\
&\ddot{x}_{\mathrm{c}} m_{\mathrm{c}} + \widetilde{k}_{42} x_{\mathrm{I}} + \widetilde{k}_{44} x_{\mathrm{c}} + \widetilde{k}_{45} x_{\mathrm{m}} + \widetilde{c}_{42} \dot{x}_{\mathrm{I}} + \widetilde{c}_{44} \dot{x}_{\mathrm{c}} \\
&+ \widetilde{c}_{45} \dot{x}_{\mathrm{m}} - \widetilde{\gamma}_{24} (x_{\mathrm{I}} - x_{\mathrm{c}})^3 - \widetilde{\beta}_{45} (x_{\mathrm{c}} - x_{\mathrm{m}})^2 \\
&+ \widetilde{\gamma}_{45} (x_{\mathrm{c}} - x_{\mathrm{m}})^3 = 0, \\
&\ddot{x}_{\mathrm{m}} m_{\mathrm{m}} + \widetilde{k}_{54} x_{\mathrm{c}} + \widetilde{k}_{55} x_{\mathrm{m}} + \widetilde{c}_{54} \dot{x}_{\mathrm{c}} + \widetilde{c}_{55} \dot{x}_{\mathrm{m}} \\
&+ \widetilde{\beta}_{45} (x_{\mathrm{c}} - x_{\mathrm{m}})^2 - \widetilde{\gamma}_{45} (x_{\mathrm{c}} - x_{\mathrm{m}})^3 = P \cos(\omega t),
\end{aligned}
\tag{1}
$$

where

$$
\begin{aligned}
&\widetilde{k}_{11} = k_{\mathrm{TM}} + k_{\mathrm{AML}} + k_{\mathrm{IMJ}}, \widetilde{k}_{12} = -k_{\mathrm{IMJ}}, \\
&\widetilde{c}_{11} = c_{\mathrm{TM}} + c_{\mathrm{AML}} + c_{\mathrm{IMJ}}, \widetilde{c}_{12} = -c_{\mathrm{IMJ}}, \\
&\widetilde{k}_{21} = \widetilde{k}_{12}, \widetilde{k}_{22} = k_{\mathrm{PIL}} + k_{\mathrm{ISJ}} + k_{\mathrm{IMJ}} + k_{\mathrm{clip}}, \\
&\widetilde{k}_{23} = -k_{\mathrm{ISJ}}, \widetilde{k}_{24} = -k_{\mathrm{clip}}, \widetilde{\gamma}_{24} = k_{\mathrm{clip3}}, \\
&\widetilde{c}_{21} = -c_{\mathrm{IMJ}}, \widetilde{c}_{22} = c_{\mathrm{PIL}} + c_{\mathrm{ISJ}} + c_{\mathrm{IMJ}} + c_{\mathrm{clip}}, \\
&\widetilde{c}_{23} = -c_{\mathrm{ISJ}}, \widetilde{c}_{24} = -c_{\mathrm{clip}}, \widetilde{k}_{32} = \widetilde{k}_{23}, \widetilde{k}_{33} = k_{\mathrm{AL}} + k_{\mathrm{ISJ}} + k_{\mathrm{C}}, \\
&\widetilde{c}_{32} = \widetilde{c}_{23}, \widetilde{c}_{33} = c_{\mathrm{AL}} + c_{\mathrm{ISJ}} + c_{\mathrm{C}}, \widetilde{\gamma}_{3} = k_{\mathrm{AL3}}, \widetilde{k}_{42} = \widetilde{k}_{24}, \\
&\widetilde{k}_{44} = k_{\mathrm{clip}} + k_{\mathrm{m}}, \widetilde{k}_{45} = -k_{\mathrm{m}}, \widetilde{c}_{42} = \widetilde{c}_{24}, \widetilde{c}_{44} = c_{\mathrm{clip}} + c_{\mathrm{m}}, \\
&\widetilde{c}_{45} = -c_{\mathrm{m}}, \widetilde{\gamma}_{45} = k_{\mathrm{m3}}, \widetilde{\beta}_{45} = k_{\mathrm{m2}}, \widetilde{k}_{54} = \widetilde{k}_{45}, \\
&\widetilde{k}_{55} = k_{\mathrm{m}} = -\widetilde{k}_{54}, \widetilde{c}_{54} = \widetilde{c}_{45}, \widetilde{c}_{55} = c_{\mathrm{m}} = -\widetilde{c}_{54}.
\end{aligned}
\tag{2}
$$

Next, the dimensionless time τ, frequency Ω, and coordinates $x_1 - x_5$ are introduced according to the following expressions:

$$
\begin{aligned}
&\tau = \omega_0 t, \omega_0 = \sqrt{\frac{k_{\mathrm{AML}}}{m_{\mathrm{M}}}}, x_1 = \frac{x_{\mathrm{M}}}{x_{\mathrm{st}}}, x_2 = \frac{x_{\mathrm{I}}}{x_{\mathrm{st}}}, \\
&x_3 = \frac{x_{\mathrm{S}}}{x_{\mathrm{st}}}, x_4 = \frac{x_{\mathrm{c}}}{x_{\mathrm{st}}}, x_5 = \frac{x_{\mathrm{m}}}{x_{\mathrm{st}}}.
\end{aligned}
\tag{3}
$$

The dimensionless equations of motion take the form

$$
\begin{aligned}
&\ddot{x}_1 + k_{11} x_1 + k_{12} x_2 + c_{11} \dot{x}_1 + c_{12} \dot{x}_2 = q \cos(\Omega \tau), \\
&\ddot{x}_2 m_2 + k_{21} x_1 + k_{22} x_2 + k_{23} x_3 + k_{24} x_4 + c_{21} \dot{x}_1 \\
&\quad + c_{22} \dot{x}_2 + c_{23} \dot{x}_3 + c_{24} \dot{x}_4 + \gamma_{24} (x_2 - x_4)^3 = 0, \\
&\ddot{x}_3 m_3 + k_{32} x_2 + k_{33} x_3 + c_{32} \dot{x}_2 + c_{33} \dot{x}_3 + \gamma_3 x_3^3 = 0, \\
&\ddot{x}_4 m_4 + k_{42} x_2 + k_{44} x_4 + k_{45} x_5 + c_{42} \dot{x}_2 + c_{44} \dot{x}_4 \\
&\quad + c_{45} \dot{x}_5 - \gamma_{24} (x_2 - x_4)^3 - \beta_{45} (x_4 - x_5)^2 \\
&+ \gamma_{45} (x_4 - x_5)^3 = 0, \\
&\ddot{x}_5 m_5 + k_{54} x_4 + k_{55} x_5 + c_{54} \dot{x}_4 + c_{55} \dot{x}_5 \\
&\quad + \beta_{45} (x_4 - x_5)^2 - \gamma_{45} (x_4 - x_5)^3 = p \cos(\Omega \tau),
\end{aligned}
\tag{4}
$$

where dimensionless parameters are defined as follows:

$$
\begin{aligned}
&k_{11} = \frac{\widetilde{k}_{11}}{(m_{\mathrm{M}} \omega_0^2)}, k_{12} = \frac{\widetilde{k}_{12}}{(m_{\mathrm{M}} \omega_0^2)}, c_{11} = \frac{\widetilde{c}_{11}}{(m_{\mathrm{M}} \omega_0)}, \\
&c_{12} = \frac{\widetilde{c}_{12}}{(m_{\mathrm{M}} \omega_0)}, k_{21} = \frac{\widetilde{k}_{21}}{(m_{\mathrm{M}} \omega_0^2)}, k_{22} = \frac{\widetilde{k}_{22}}{(m_{\mathrm{M}} \omega_0^2)}, \\
&k_{23} = \frac{\widetilde{k}_{23}}{(m_{\mathrm{M}} \omega_0^2)}, k_{24} = \frac{\widetilde{k}_{24}}{(m_{\mathrm{M}} \omega_0^2)}, c_{21} = \frac{\widetilde{c}_{21}}{(m_{\mathrm{M}} \omega_0)}, \\
&c_{22} = \frac{\widetilde{c}_{22}}{(m_{\mathrm{M}} \omega_0)}, c_{23} = \frac{\widetilde{c}_{23}}{(m_{\mathrm{M}} \omega_0)}, c_{24} = \frac{\widetilde{c}_{24}}{(m_{\mathrm{M}} \omega_0)}, \\
&\gamma_{24} = \frac{\widetilde{\gamma}_{24} x_{\mathrm{st}}^2}{(m_{\mathrm{M}} \omega_0^2)}, k_{32} = \frac{\widetilde{k}_{32}}{(m_{\mathrm{M}} \omega_0^2)}, k_{33} = \frac{\widetilde{k}_{33}}{(m_{\mathrm{M}} \omega_0^2)}, \\
&c_{32} = \frac{\widetilde{c}_{32}}{(m_{\mathrm{M}} \omega_0)}, c_{33} = \frac{\widetilde{c}_{33}}{(m_{\mathrm{M}} \omega_0)}, \gamma_3 = \frac{\widetilde{\gamma}_3 x_{\mathrm{st}}^2}{(m_{\mathrm{M}} \omega_0^2)}, \\
&k_{42} = \frac{\widetilde{k}_{42}}{(m_{\mathrm{M}} \omega_0^2)}, k_{44} = \frac{\widetilde{k}_{44}}{(m_{\mathrm{M}} \omega_0^2)}, k_{45} = \frac{\widetilde{k}_{45}}{(m_{\mathrm{M}} \omega_0^2)}, \\
&c_{42} = \frac{\widetilde{c}_{42}}{(m_{\mathrm{M}} \omega_0)}, c_{44} = \frac{\widetilde{c}_{44}}{(m_{\mathrm{M}} \omega_0)}, c_{45} = \frac{\widetilde{c}_{45}}{(m_{\mathrm{M}} \omega_0)}, \\
&\gamma_{45} = \frac{\widetilde{\gamma}_{45} x_{\mathrm{st}}^2}{(m_{\mathrm{M}} \omega_0^2)}, \beta_{45} = \frac{\widetilde{\beta}_{45} x_{\mathrm{st}}}{(m_{\mathrm{M}} \omega_0^2)}, k_{54} = \frac{\widetilde{k}_{54}}{(m_{\mathrm{M}} \omega_0^2)}, \\
&k_{55} = \frac{\widetilde{k}_{55}}{(m_{\mathrm{M}} \omega_0^2)}, c_{54} = \frac{\widetilde{c}_{54}}{(m_{\mathrm{M}} \omega_0)}, c_{55} = \frac{\widetilde{c}_{55}}{(m_{\mathrm{M}} \omega_0)}, \\
&\omega = \Omega \omega_0, q = \frac{Q}{(m_{\mathrm{M}} x_{\mathrm{st}} \omega_0^2)}, p = \frac{P}{(m_{\mathrm{M}} x_{\mathrm{st}} \omega_0^2)}.
\end{aligned}
\tag{5}
$$

The implant can be used in various types of hearing loss. Here, it is assumed that sound does not reach to the malleus ($q = 0$) and therefore the incus is stimulated only by the transducer ($p \neq 0$). Properties of the transducer are important to obtain satisfactory middle ear characteristics; therefore, stiffness $k_{\mathrm{CLIP}}, k_{\mathrm{m}}$, and mass of the can and the

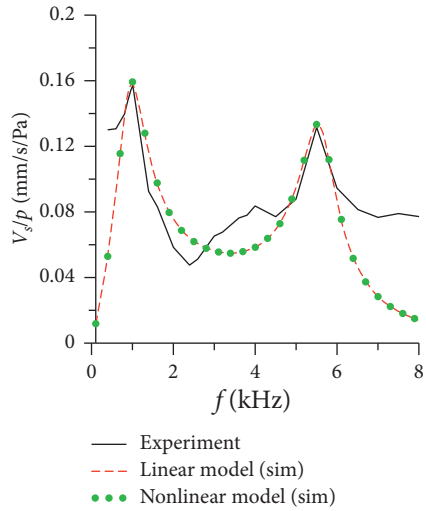

FIGURE 3: Transfer function of the stapes vibration for numerical (3dof model) and experimental results.

magnet (M_m, M_c) are significant and will be analysed first in Section 4.

The middle ear model with the transducer has stronger capacity to dissipate energy than the normal ear. Dissipated energy can be defined by Rayleigh's dissipation function D that is expressed for the implanted ear by the equation

$$D_{FMT} = D_{NME} + \frac{1}{2}c_{CLIP}\left(\dot{x}_I - \dot{x}_c\right)^2 + \frac{1}{2}c_m\left(\dot{x}_c - \dot{x}_m\right)^2, \quad (6)$$

where D_{NME} means the dissipated energy for the normal middle ear, defined as follows:

$$D_{NME} = \frac{1}{2}c_{AML}\dot{x}_M^2 + \frac{1}{2}c_{IMJ}\left(\dot{x}_M - \dot{x}_I\right)^2 + \frac{1}{2}c_{PIL}\dot{x}_I^2 + \frac{1}{2}c_{ISJ}\left(\dot{x}_I - \dot{x}_S\right)^2 + \frac{1}{2}\left(c_{AL} + c_C\right)\dot{x}_S^2. \quad (7)$$

Stronger energy dissipation in the IME has to be compensated by more powerful stimulation.

3. Dynamics of Normal Middle Ear

The three-degree-of-freedom model of the normal middle ear, proposed here, is verified by an experiment on a human temporal bone. Research has been performed using a laser Doppler vibrometer (LDV). The experimental rig and methodology of experimental procedure are described in [13, 14, 15]. Numerical results of the 3dof system, both linear and nonlinear, are convergent with the experiment. This is presented as the transfer function between sound pressure and stapes velocity in Figure 3. Both numerical results obtained on the basis of linear and nonlinear 3dof model are consistent with experimental outcomes. This proves that the 3dof model of the intact (normal) middle ear is correctly developed. Nonlinearities presented in the model could be neglected here, but in the case of more complicated system or different conditions, they could be important. Vibration amplitudes can vary depending on individual patient's features, but resonance peaks should be almost at the same frequencies. This is shown in the results of experiments made by several authors, which are compared in the paper [14]. The transducer is a new element in the middle ear structure that can change a middle ear characteristic. Therefore, the transducer should be chosen in the proper way to obtain characteristics of the ear with the implant similar to the NME. At the beginning, natural frequencies and vibration modes of the 3dof linear model are shown in Figure 4, while the response of the nonlinear system is presented in Figures 5 and 6 as resonance curves (bold lines) for parameters presented in Table 1. The parameters of the middle ear are taken from [14, 16, 17]. However, nonlinearity of the annular ligament and the silicon rubber are taken from [10, 11], respectively. The standard damping parameters (c) characterize the healthy ear (Figure 5) while decreased ones (c_1) represent the pathological ear (Figure 6). Figure 5 also shows the resonance curves of the 5dof system (thin lines) that will be discussed later in the following section. Dimensionless natural frequencies of the linear system shown in Figure 4 correspond to real (dimensional) frequencies of 0.97 kHz, 5.59 kHz, and 43.8 kHz. The middle ear behaves as a linear oscillator near the first resonance because nonlinearity is weak for small oscillation amplitude observed in the human ear. Even decrease in damping does not visualize any nonlinear effects in the system response. Interestingly, the second resonance is characterized by a nonsymmetric curve due to nonlinearity of the annular ligament.

4. Dynamics of Implanted Middle Ear

Placing an implant to the ear structure, dynamics of the middle ear can change because of additional mass and nonlinear properties of a transducer. Therefore, at the beginning, linear analysis of the middle ear with the implant (5dof) is performed to estimate basic transducer parameters. Next, the nonlinear model of the IME is engaged to explore full dynamics of the system.

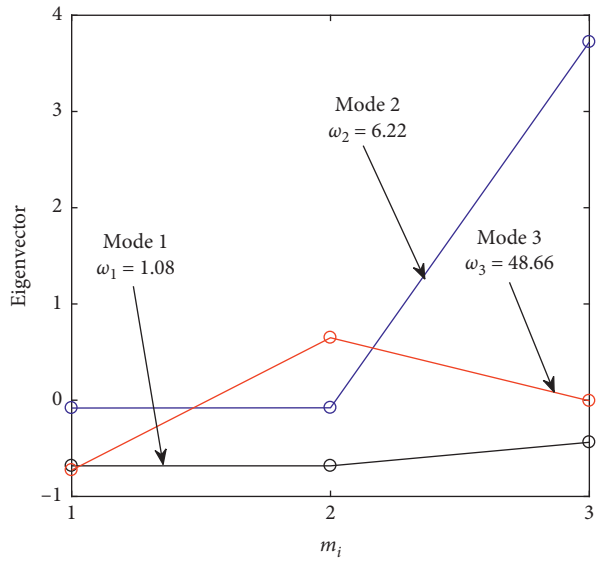

Figure 4: Modes of the 3dof model of the normal middle ear.

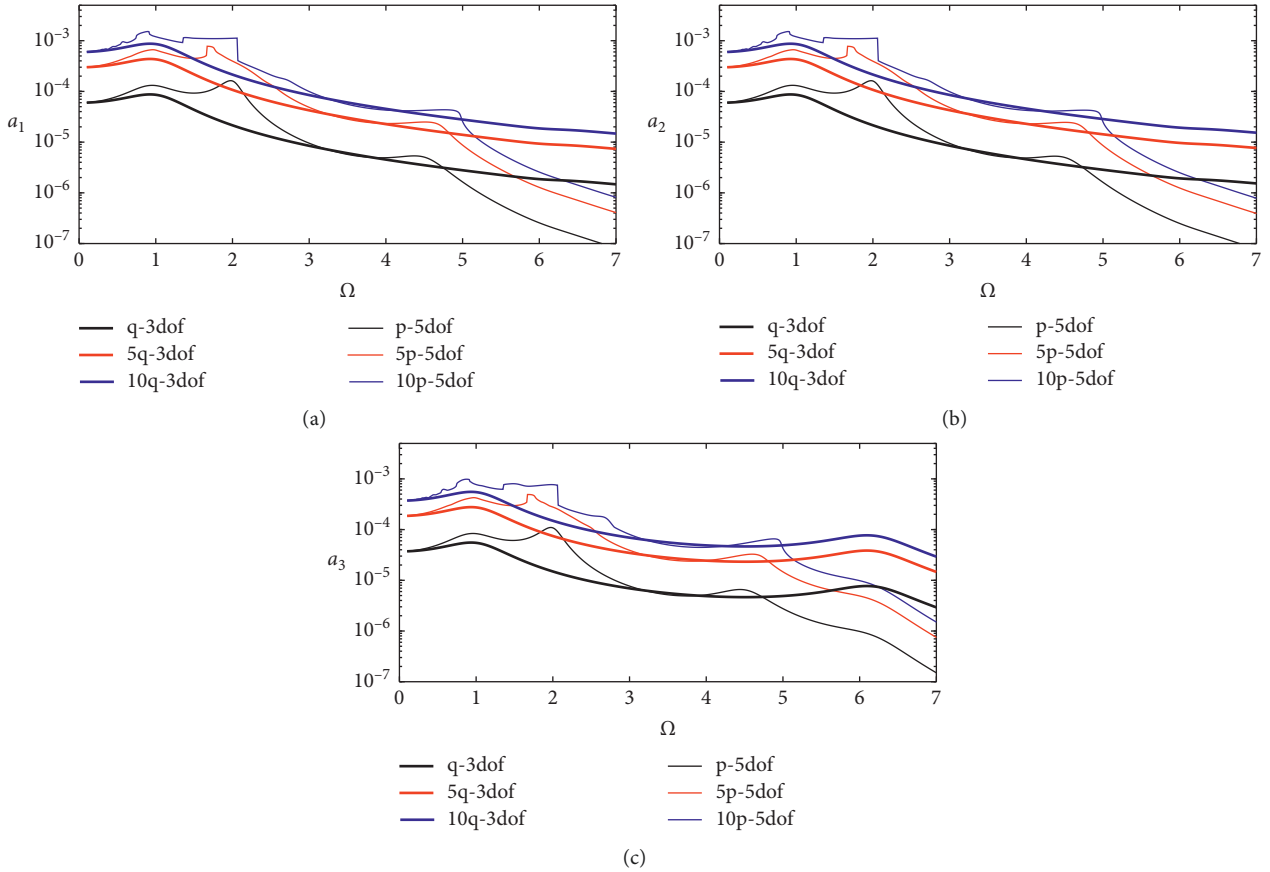

Figure 5: Resonance curves of the normal ear, modelled as the 3dof and 5dof system: the malleus (a), the incus (b), and the stapes (c).

4.1. Linear Model. Analysis of the linear 5dof model is performed for parameters from Table 1. However, different variants of the transducer and the coupler (clip) properties are investigated here in order to find the proper ones. The stiffness ratio of silicon spring and the clip (k_m/k_{CLIP}) is confronted with the mass ratio between the magnet and the can (m_5/m_4). An influence of the stiffness and the mass ratio on natural frequencies of the implanted middle ear is presented in Figure 7. Numerical analysis of the NME and also experimental research reported in [7, 8, 14, 18, 19] show that the first and second natural frequencies are about 1 kHz and 5 kHz, respectively. To get similar values of natural

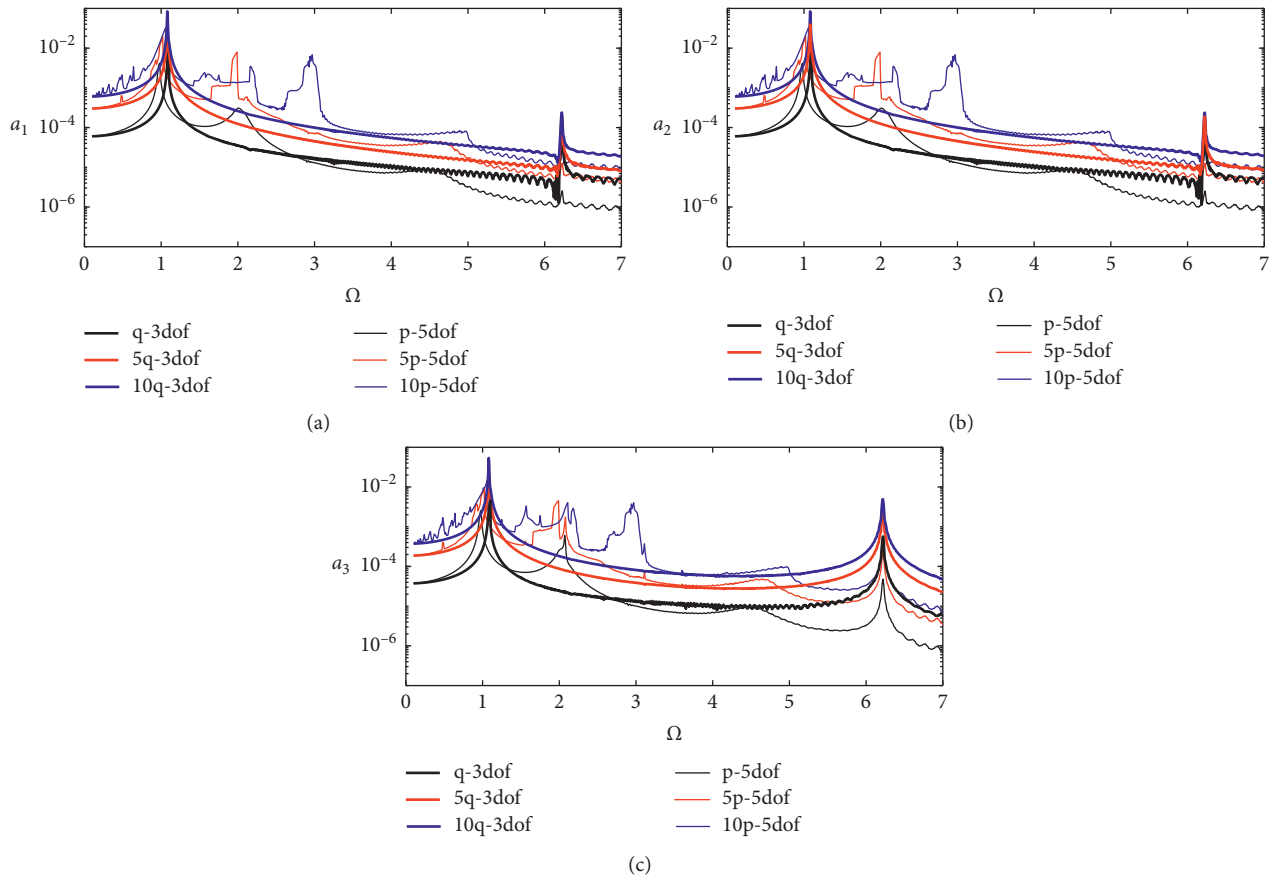

Figure 6: Resonance curves of the pathological ear, modelled as the 3dof and 5dof system: the malleus (a), the incus (b), and the stapes (c).

Table 1: Parameters of the middle ear model.

Mass, m (mg)	k (mN/μm)	c (mNs/mm)	k (Ns^3/mm^3)	c_1 (Ns/mm)
$m_M = 25$	$k_{TM} = 0.3$	$c_{TM} = 60$		$c_{1TM} = 0.359$
$m_I = 28$	$k_{AML} = 0.8$	$c_{AML} = 125$		$c_{1AML} = 0.538$
$m_S = 1.78$	$k_{IMJ} = 1000$	$c_{IMJ} = 359$		$c_{1IMJ} = 28.86$
$M_c = 5$	$k_{PIL} = 0.4$	$c_{PIL} = 55$		$c_{1PIL} = 0.981$
$M_m = 5$	$k_{ISJ} = 1.35$	$c_{ISJ} = 7.9$		$c_{1ISJ} = 0.039$
	$k_{AL} = 0.623$	$c_{AL} = 0.04$	$k_{AL3} = 0.013$	$c_{1AL} = 0.033$
	$k_C = 0.2$	$c_C = 1.7$	$k_{m2} = 0.188$	
	$k_m = 0.85$	$c_m = 5$	$k_{m3} = 0.014$	
	$k_{clip} = 2.0$	$c_{clip} = 10$	$k_{clip3} = 2.25$	

frequencies in case of the IME, Figure 7 should be analysed carefully considering the first and the second natural frequency. In order to obtain the proper value of the first natural frequency (ω_1) of the ear, the stiffness ratio k_m/k_{CLIP} should be greater than 0.2. In this case, the mass ratio (m_5/m_4) between 0.1 and 2 gives almost the same frequency $\omega_1 = 0.95 - 1.0$. The second natural frequency oscillates between 2 and 2.5 when $k_m/k_{CLIP} > 0.5$. As far as the third frequency (ω_3) is concerned, it changes between 2.5 and 6 in the analysed range of parameters. The fourth (ω_4) and especially the fifth (ω_5) natural frequency are much higher than the hearing range; therefore, they do not have practical meaning. The natural frequencies and modes of the linear IME are depicted in Figure 8. Mass of the can (m_c) and the magnet (m_m) have to be small enough and therefore they are assumed to be 5 mg. Then, the first (the most important) natural dimensionless frequency is 0.97. This value is very close to the frequency of the NME.

4.2. Nonlinear Model. Response of the nonlinear model of the IME (5dof) is compared to that of the 3dof model of the NME both for standard parameters (healthy ear) (Figure 5) and pathological ones (Figure 6) as a resonance curve. In Figure 5, the bold lines represent the output of the 3dof model, while the thin lines represent the 5dof one. Note that, in the 3dof system, the malleus is excited by force Q, while the 5dof system is stimulated only by the magnet of the transducer, then $Q = 0$ and $P = 0.12$ mN. Implementation of the transducer to the middle ear structure shifts the second

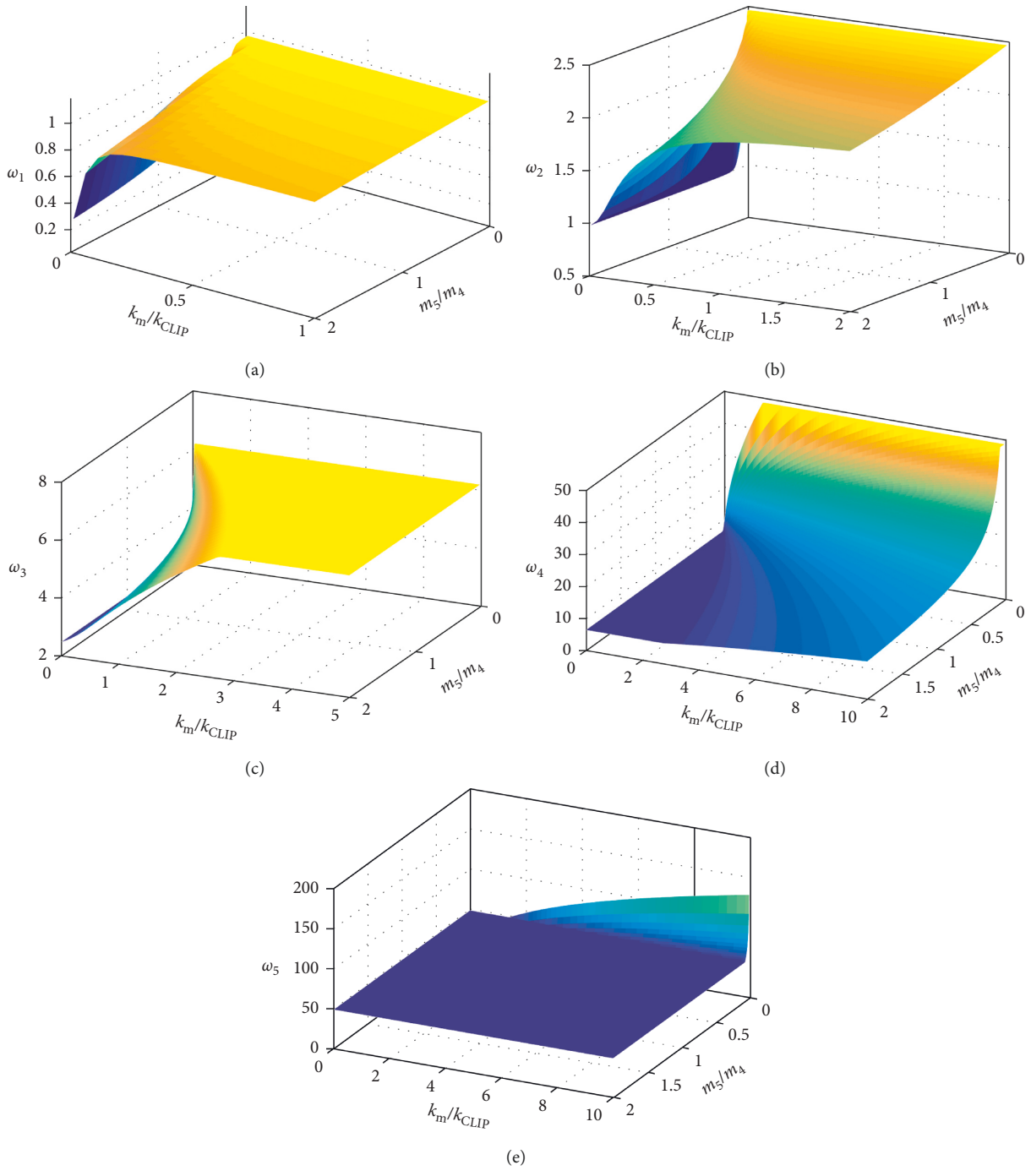

FIGURE 7: An influence of the stiffness (k_{CLIP}/k_m) and the masses (m_5/m_4) ratio on natural frequency ($\omega_1 - \omega_5$) of the middle ear system.

and the third resonance. Moreover, vibration amplitudes are bigger compared to the 3dof system. This means the transducer works well because it generates stronger effect on ossicles and amplifies sound approaching to the cochlea.

However, a strange shape of a resonance curve (with picks and plateaus) speaks for irregularity of the middle ear response, especially at low frequencies. Therefore, the detailed behaviour of the ossicles is presented as the classical Poincaré two-parameter maps (frequency Ω and amplitude p of external excitation) in Figures 9 and 10 and, moreover, in Figures 11 and 12, as bifurcation diagrams, where displacements at zero velocity are collected. The analysis of Figures 11 and 12 gives complementary knowledge to the classical Poincaré section because it is more sensitive for signal disturbance when the vibration's period is not changed. Figures 9 and 11 represent the IME for standard parameters, whereas Figures 10 and 12 for the pathological ones. The Poincaré maps (Figures 9 and 10) show the white regions of regular motion and the gray ones of irregular motion. The healthy ear (for standard

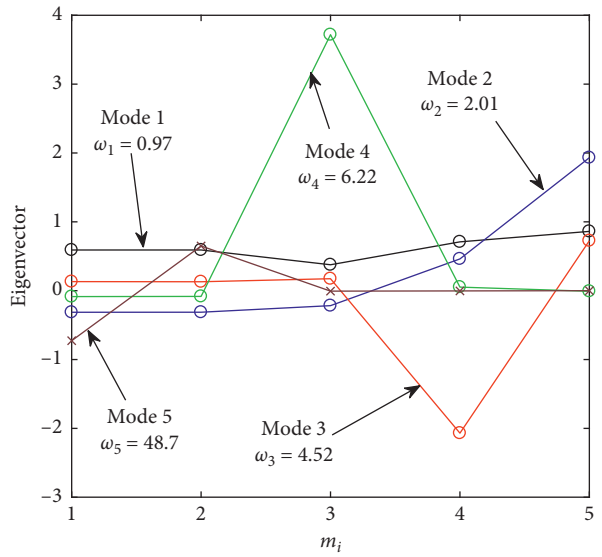

Figure 8: Modes of the 5dof model of the middle ear with implant.

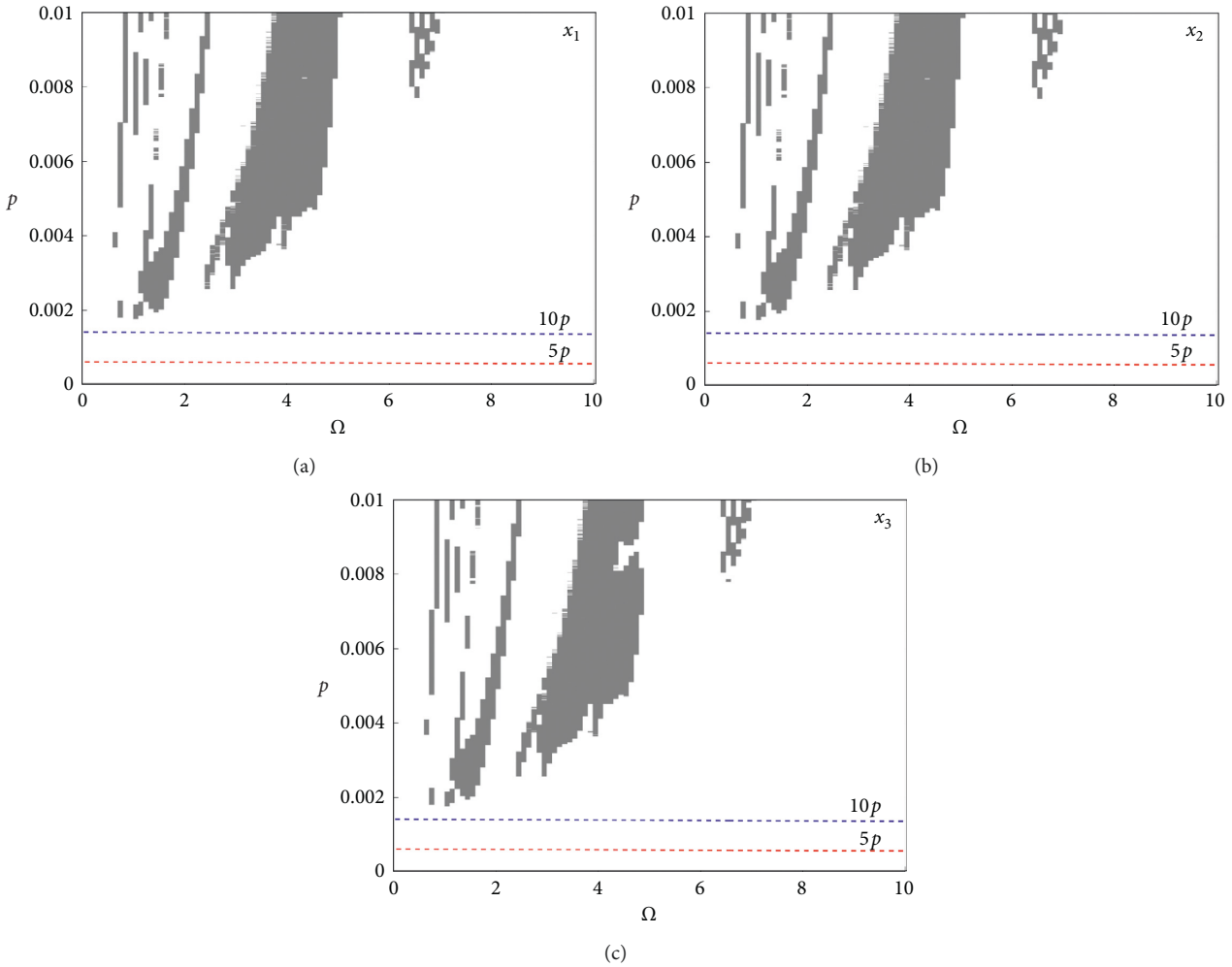

Figure 9: Poincaré map of regular and irregular motion for a healthy ear: the malleus (a), the incus (b), and the stapes (c).

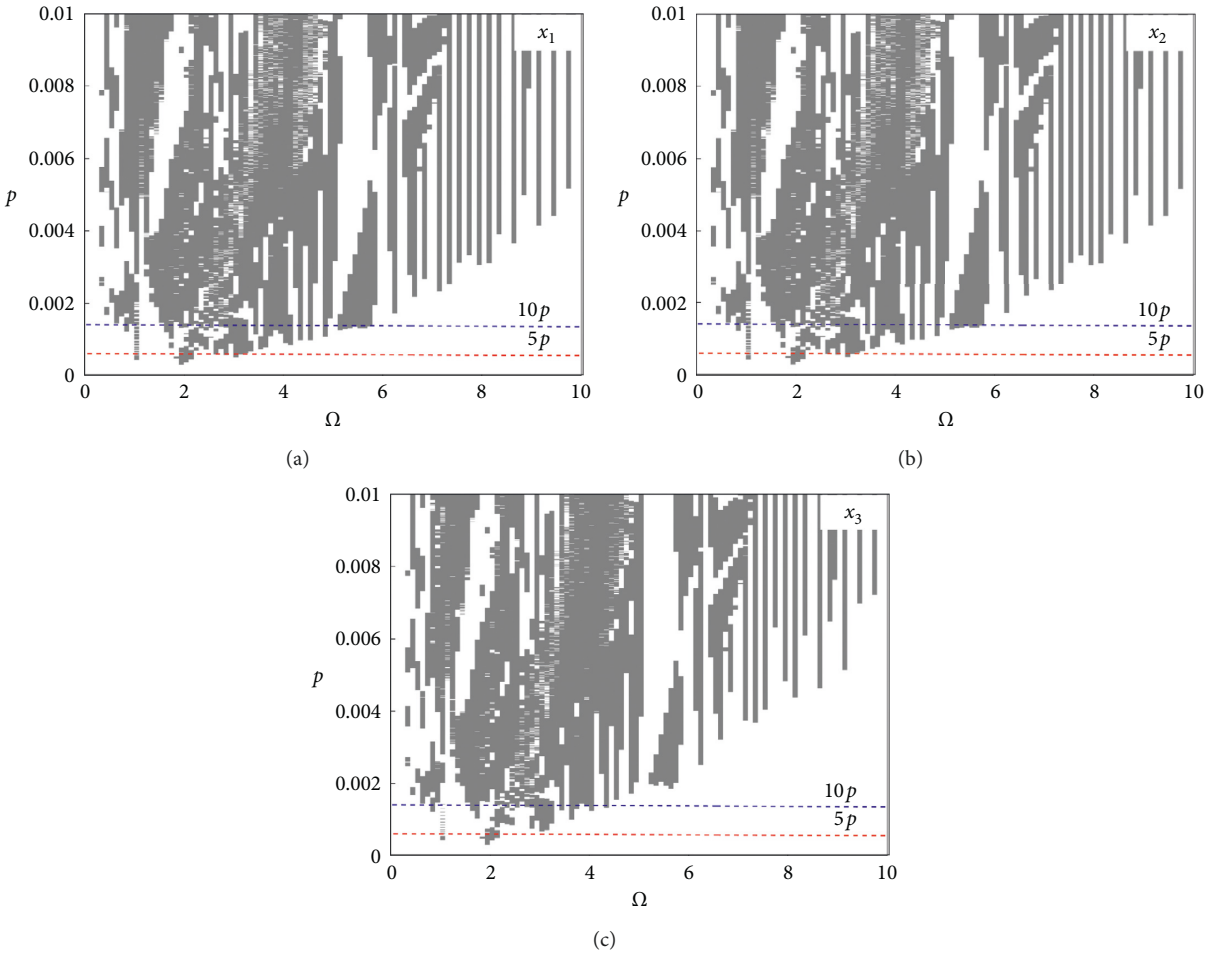

Figure 10: Poincaré map of regular and irregular motion for the pathological ear: the malleus (a), the incus (b), and the stapes (c).

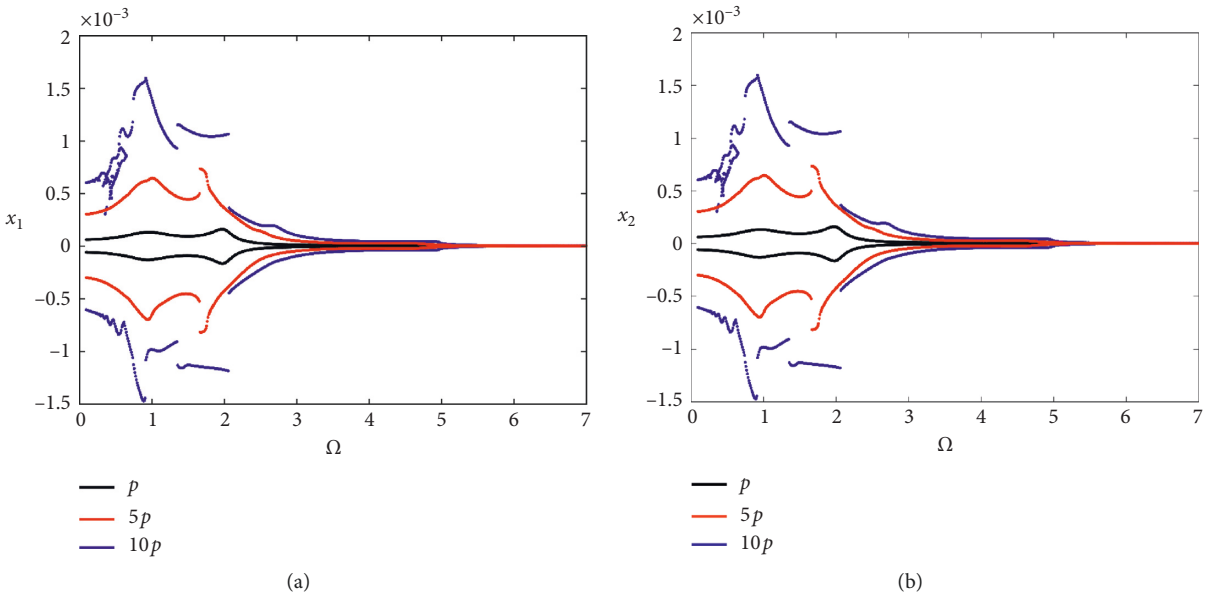

Figure 11: Continued.

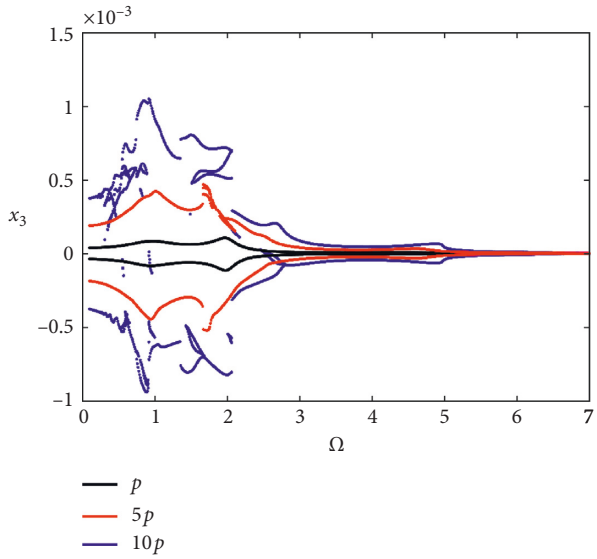

(c)

Figure 11: Bifurcation diagram at zero velocity of the healthy ear: the malleus (a), the incus (b), and the stapes (c).

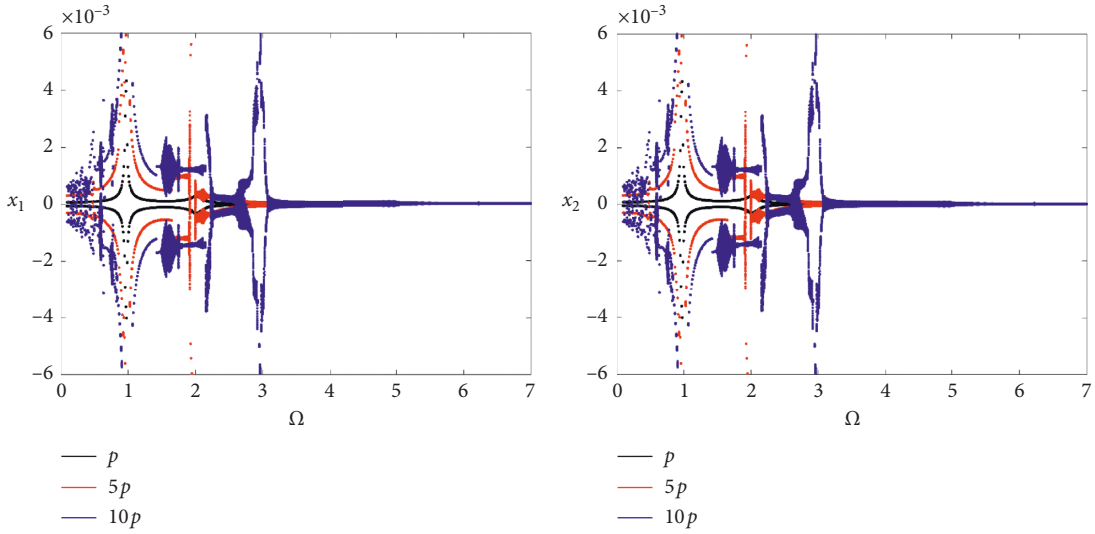

(a) (b)

Figure 12: Continued.

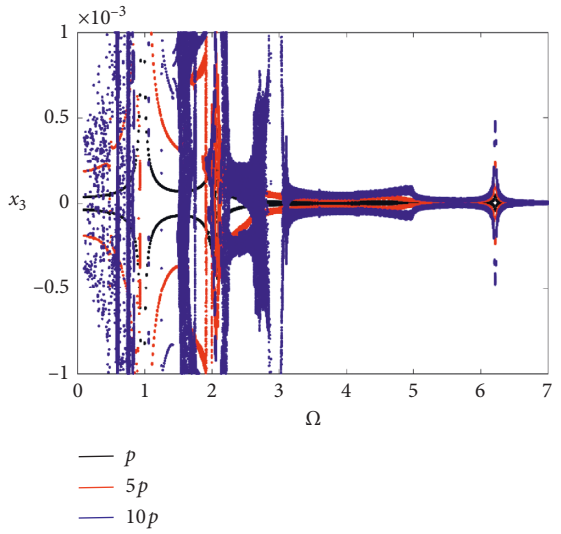

(c)

Figure 12: Bifurcation diagram at zero velocity of the pathological ear: the malleus (a), the incus (b), and the stapes (c).

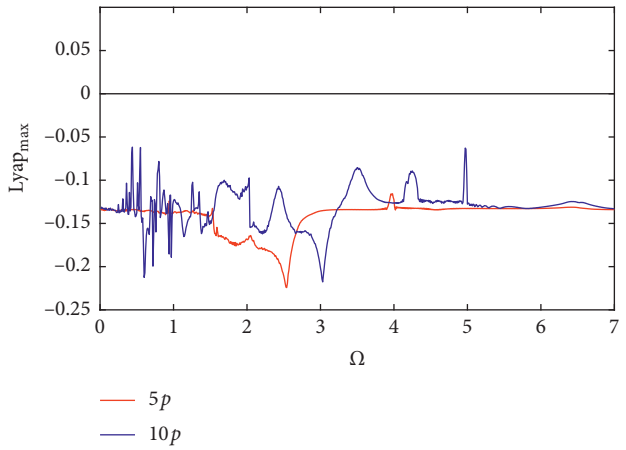

Figure 13: Maximal Lyapunov exponent of the healthy implanted middle ear.

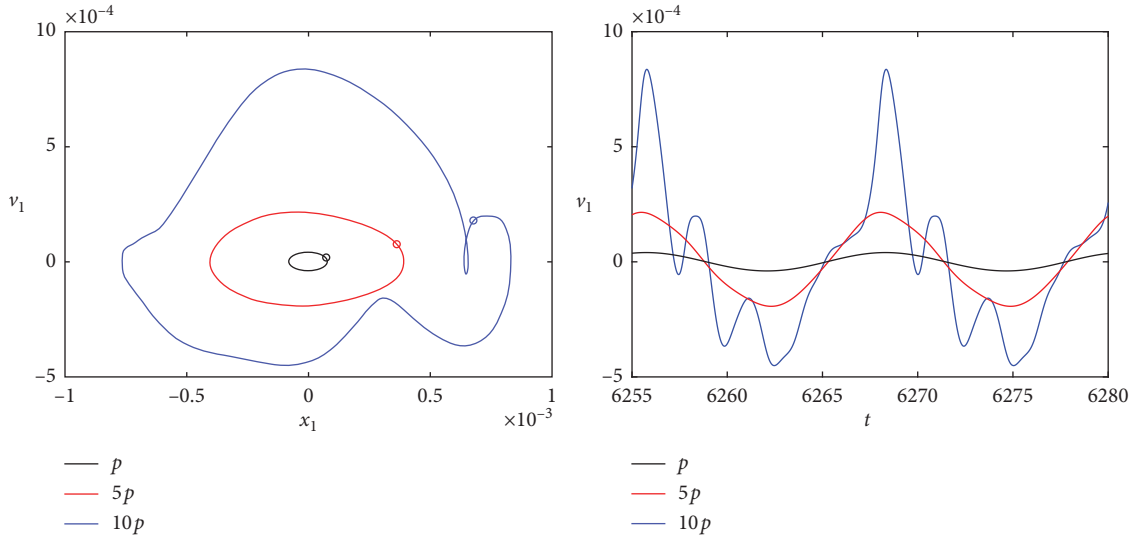

(a)

Figure 14: Continued.

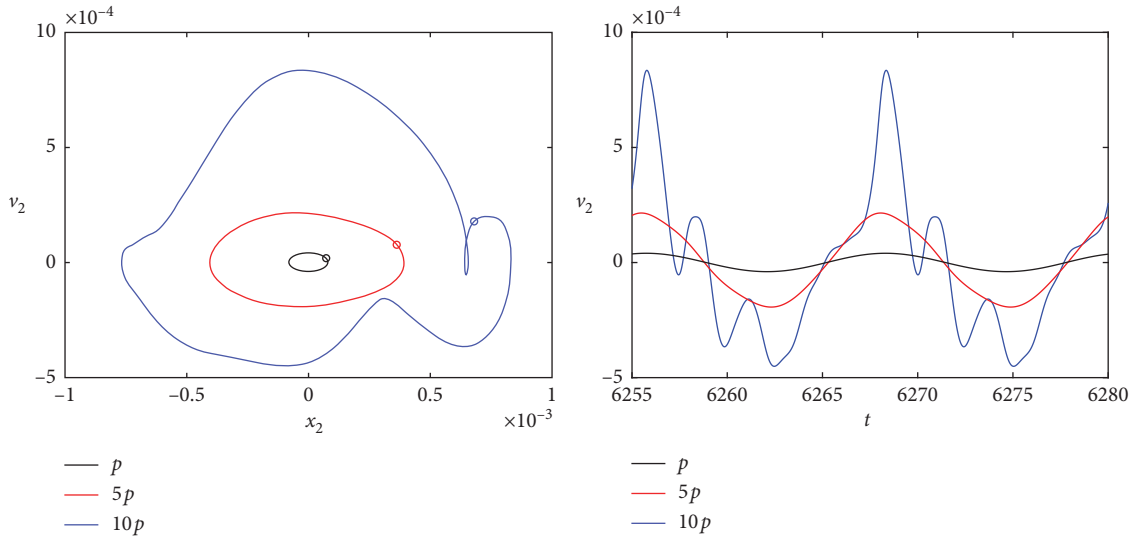

(b)

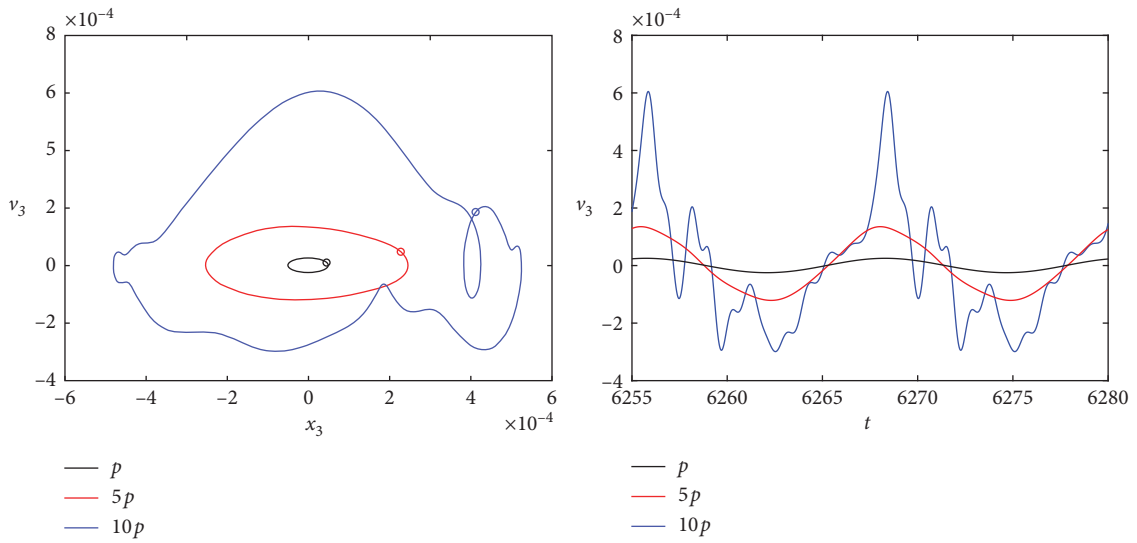

(c)

Figure 14: Phase diagram and time series of the healthy ear for $\Omega = 0.5$: the malleus (a), the incus (b), and the stapes (c).

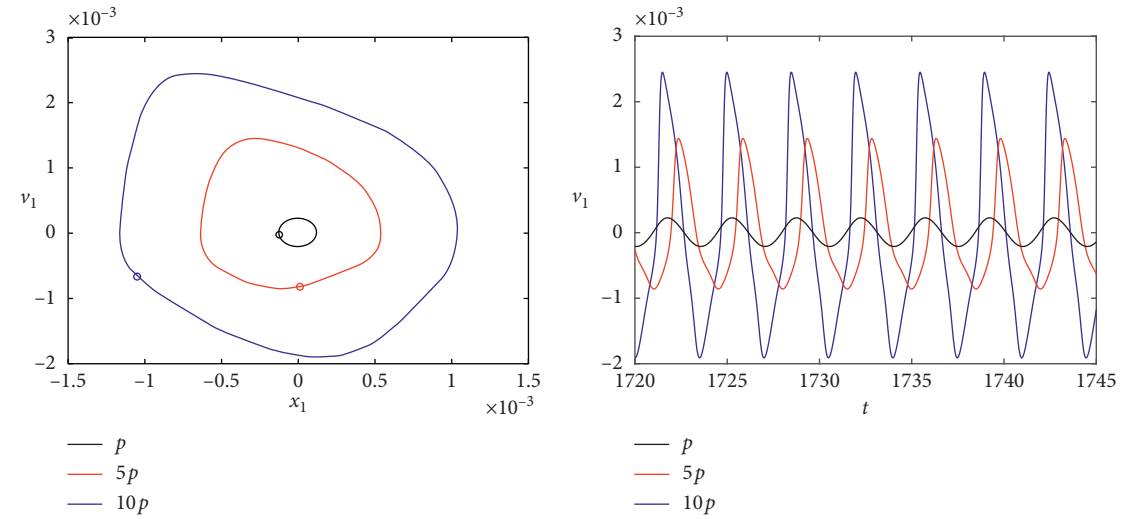

(a)

Figure 15: Continued.

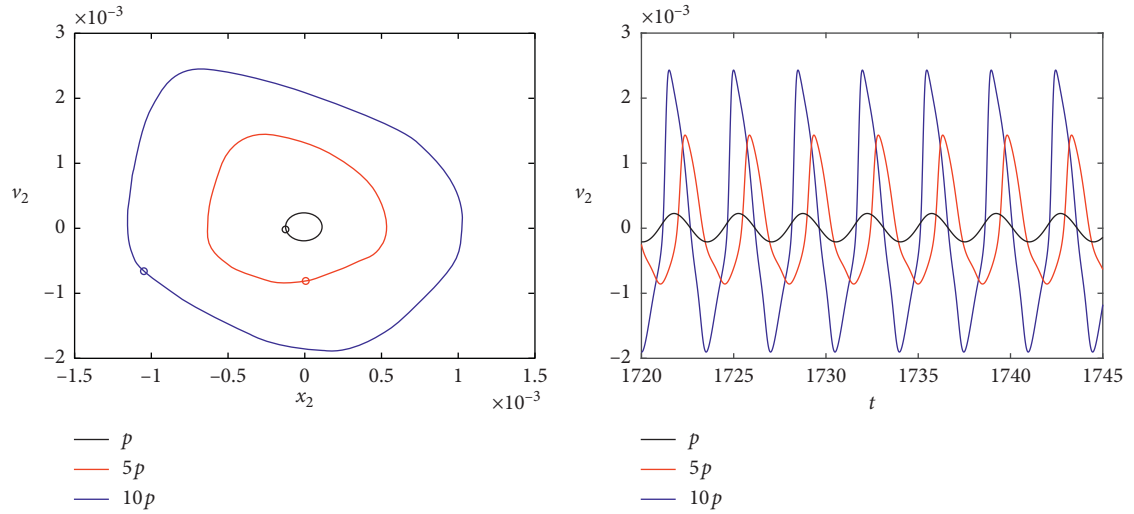

(b)

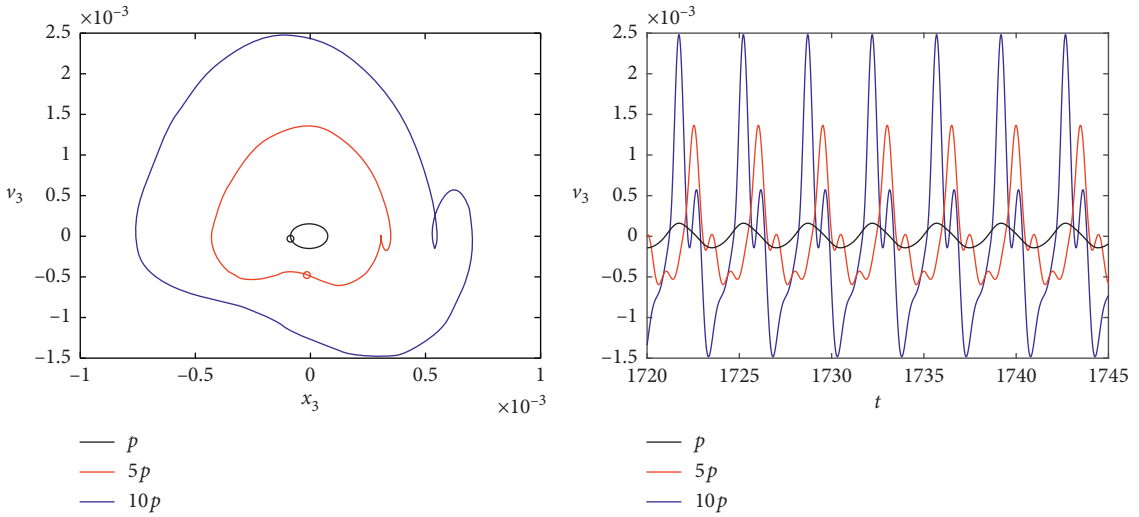

(c)

Figure 15: Phase diagram and time series of the healthy ear for $\Omega = 1.8$: the malleus (a), the incus (b), and the stapes (c).

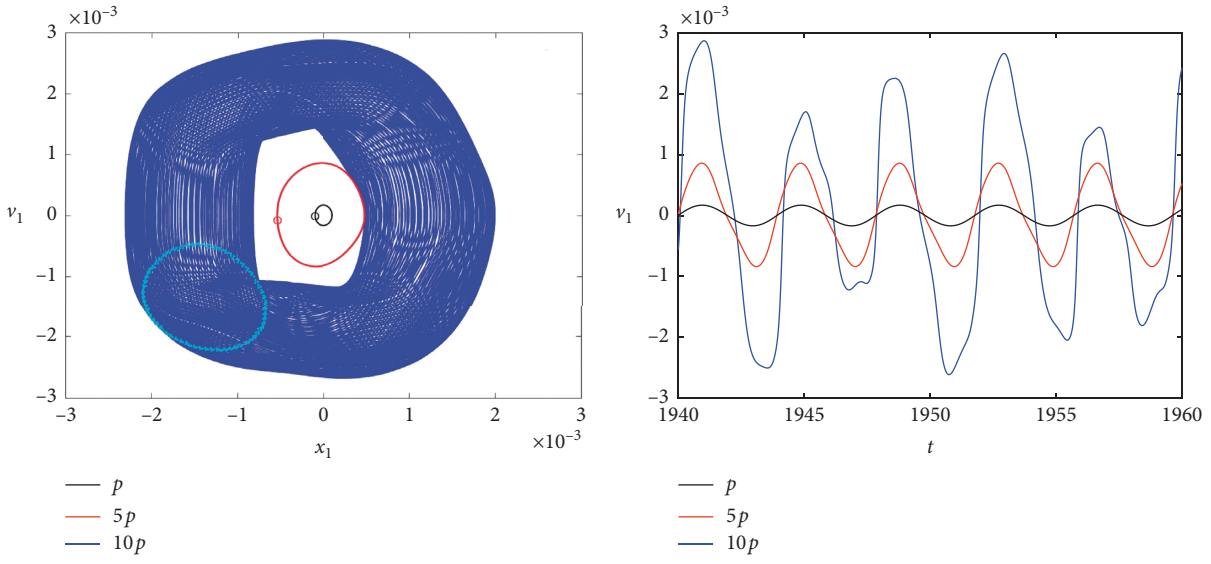

(a)

Figure 16: Continued.

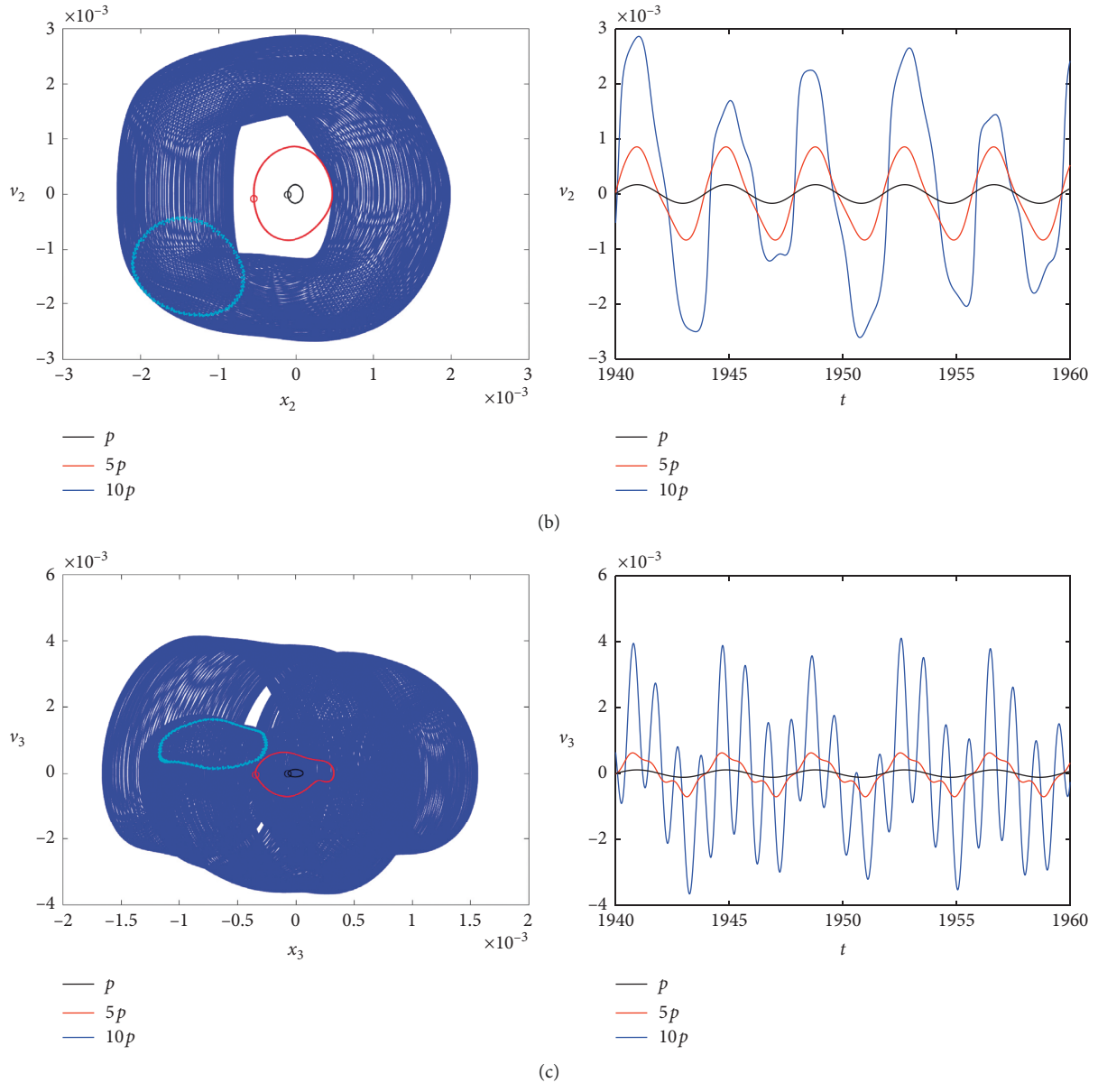

FIGURE 16: Phase diagram and time series of the pathological implanted middle ear for $\Omega = 1.6$: the malleus (a), the incus (b), and the stapes (c).

parameters) is sensitive very much for external excitation especially for amplitude $p > 0.002$. The change in excitation frequency (Ω) between 0.7 and 7 can cause chaotic behaviour of the ossicles. When the excitation amplitude $p < 0.002$, the system is unconditionally regular (the white area means regular, period 1 response). This is in agreement with the Lyapunov maximal exponent ($\text{Lyap}_{\max}$), calculated according to the Wolf algorithm for $5P$ and $10P$, presented in Figure 13. The exponent is still negative, that is, a regularity proof. The malleus (Figure 9(a)), the incus (Figure 9(b)), and the stapes (Figure 9(c)) motion are characterized by the identical gray regions. The blue and the red dashed lines represent the level of excitation corresponding to 10 and 5 times greater than the reference value (p) given in Table 1 ($P = 0.12$ mN, $p = 1.5e - 4$). The situation changes when the pathological ear with decreased damping is analysed (Figure 10). Then, the dangerous (gray) region is much wider. The unconditionally regular area exists for $p < 0.0005$, a bit below the red-dashed line. Moreover, even high frequency (Ω) does not guarantee the regular system response. Some small differences in the maps for the ossicles are noticeable. The bifurcation analysis of ossicle motion (Figure 11) is performed for three excitation amplitudes p, $5p$, and $10p$ marked by black, red, and blue colours properly. When the excitation is small (p), motion of the malleus (Figure 11(a)), the incus (Figure 11(b)), and the stapes (Figure 11(c)) is regular, while for stronger excitation ($10p$, blue colour) additional waves of different phases appear. They are presented in phase diagrams and time series of ossicle velocity in Figure 14. Circles on the trajectories represent the Poincaré points. This means the system output frequency is exactly

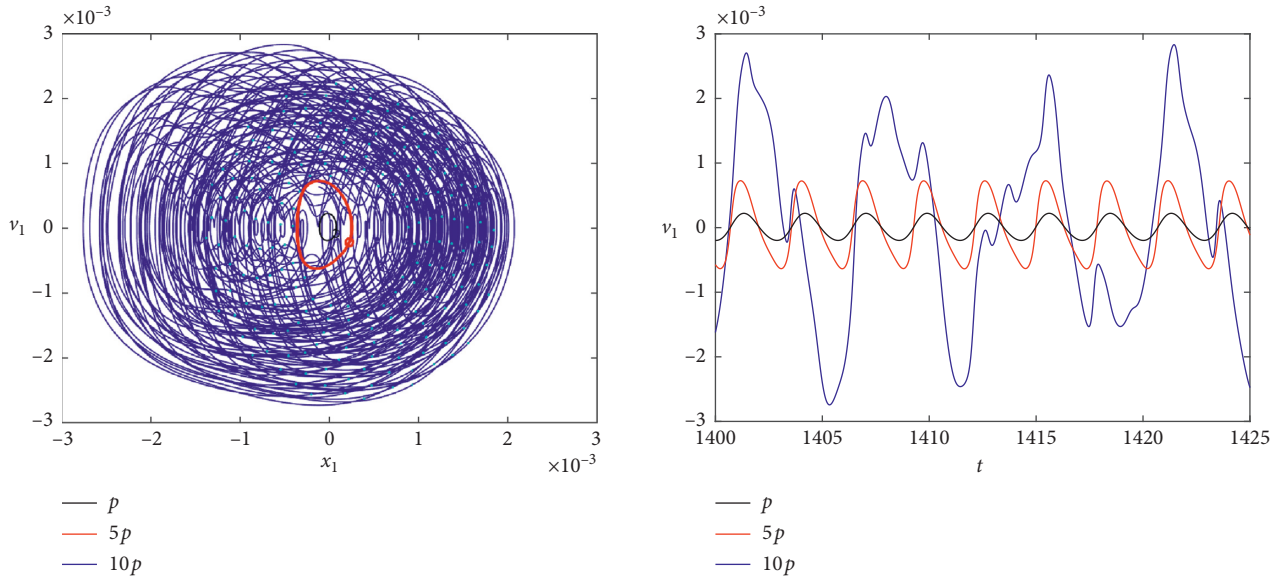

(a)

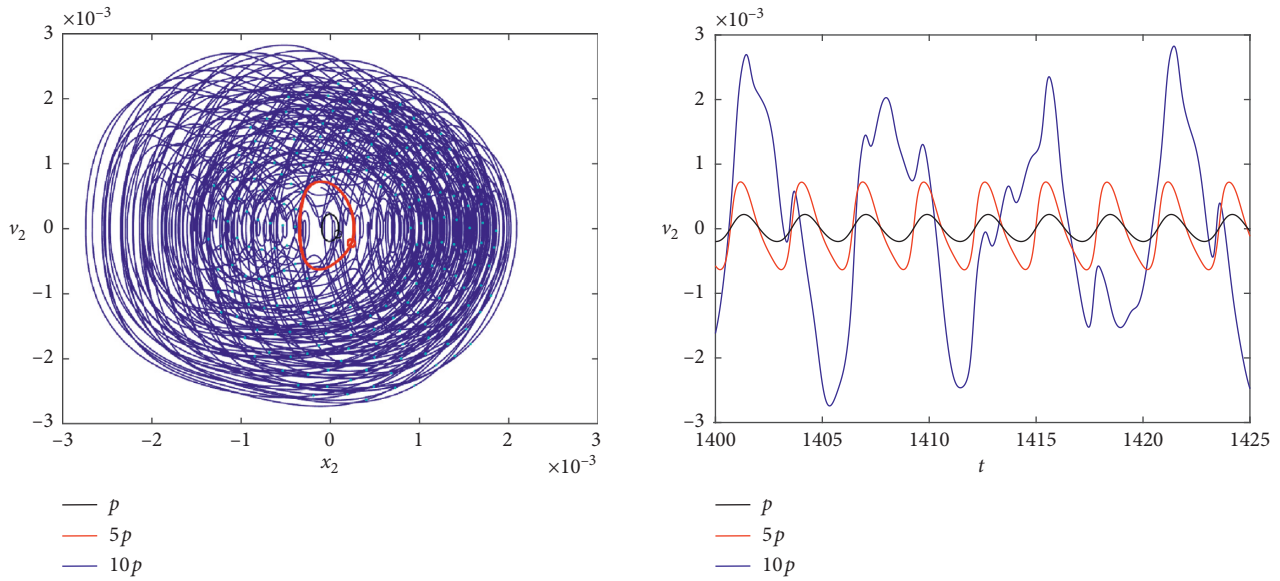

(b)

Figure 17: Continued.

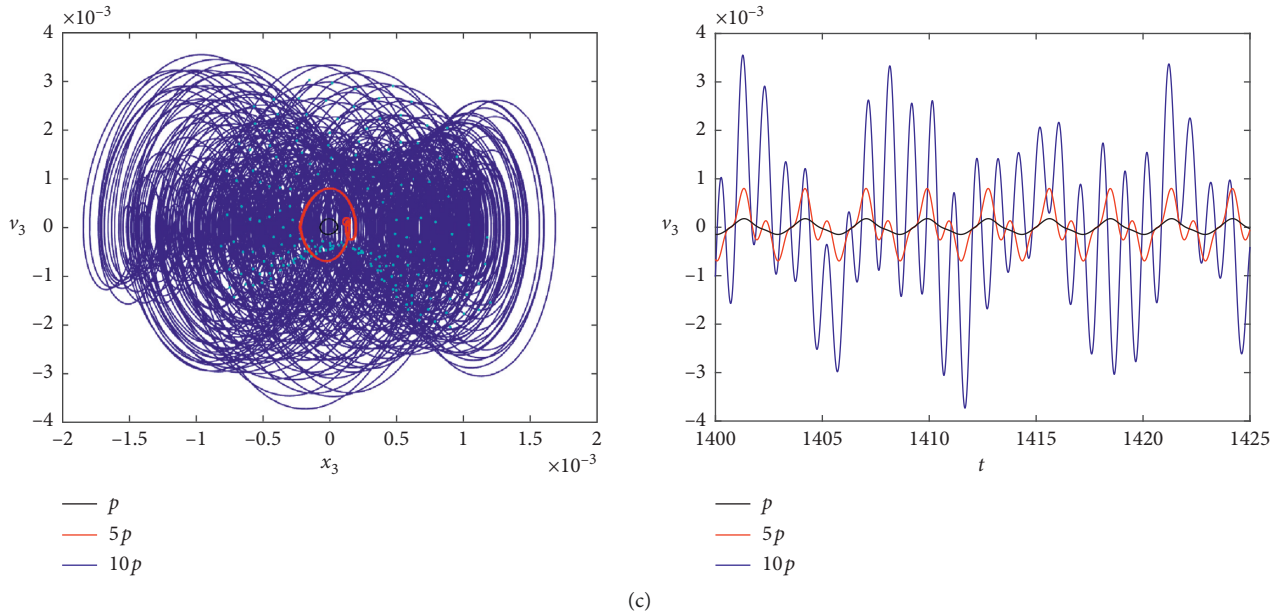

(c)

Figure 17: Phase diagram and time series of the pathological implanted middle ear for $\Omega = 2.2$: the malleus (a), the incus (b), and the stapes (c).

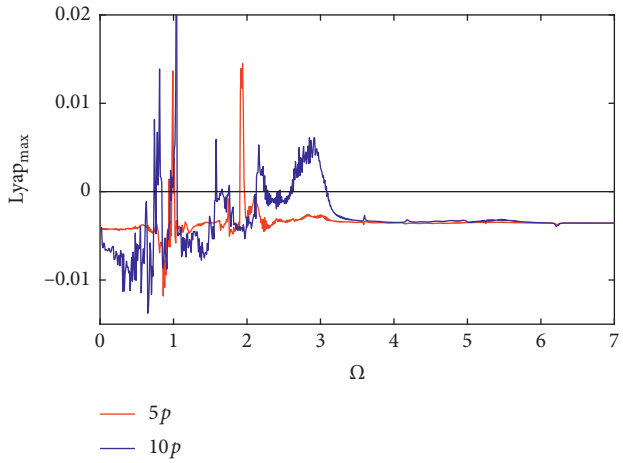

Figure 18: Maximal Lyapunov exponent of the pathological implanted middle ear.

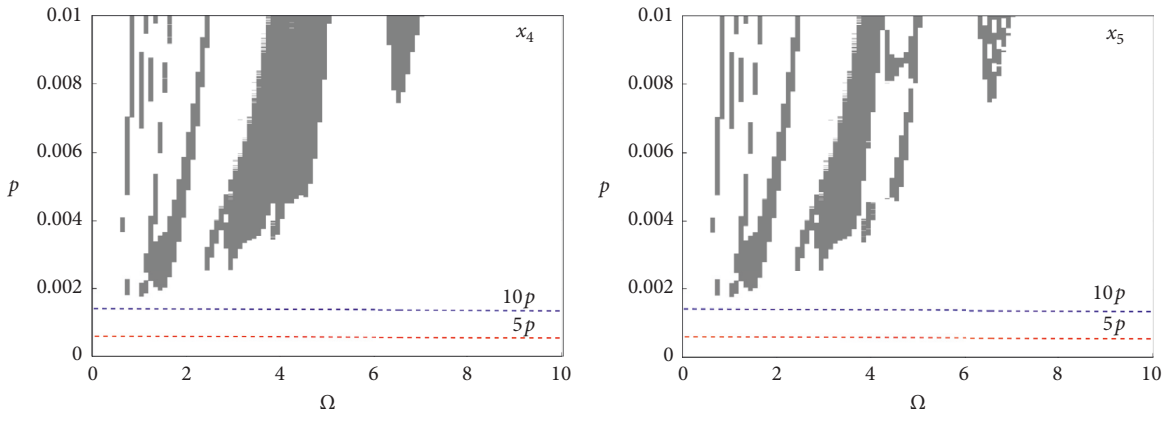

(a) (b)

Figure 19: Poincaré map of transducer regular and irregular vibrations for normal ear parameters: the can (a) and the magnet (b).

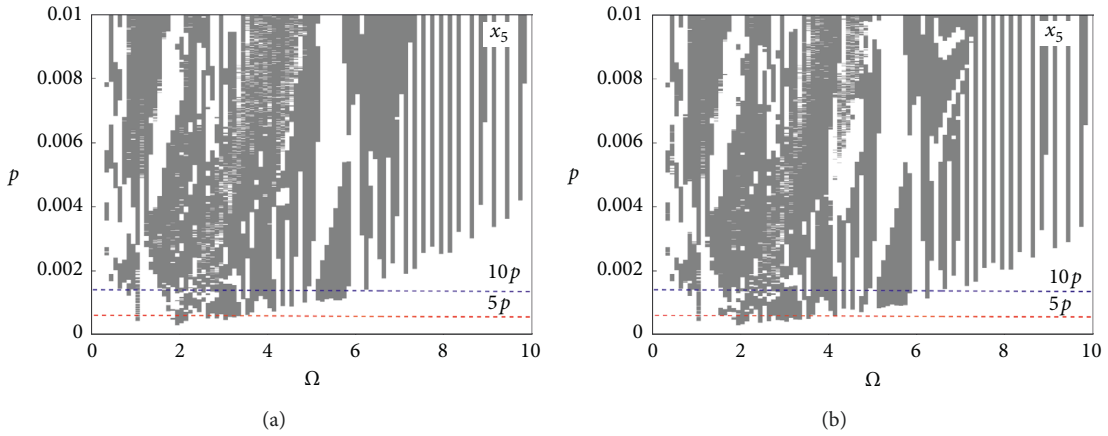

Figure 20: Poincaré map of transducer regular and irregular vibrations of the pathological ear parameters: the can (a) and the magnet (b).

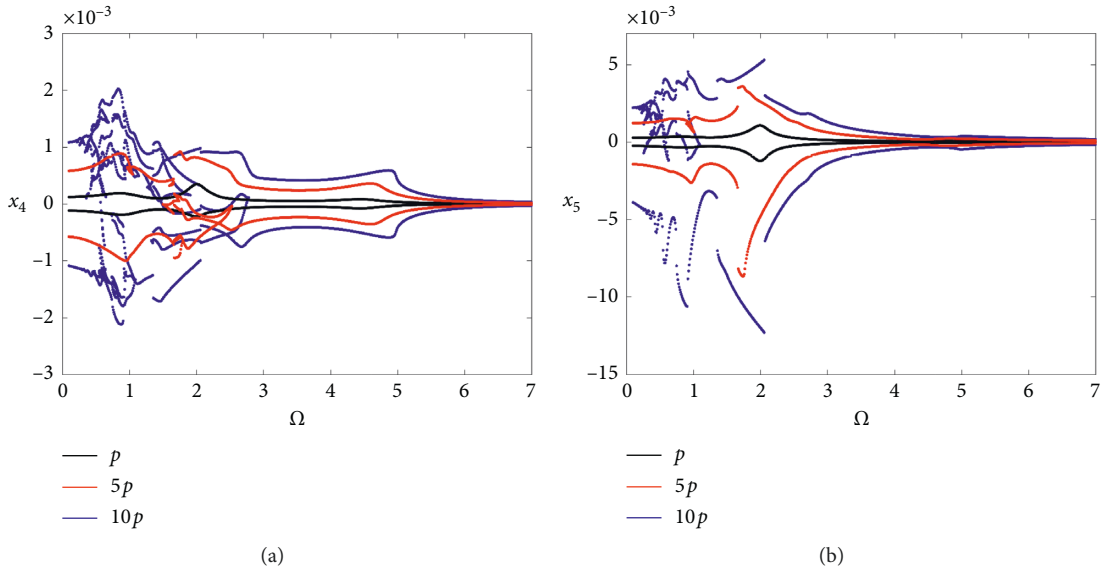

Figure 21: Bifurcation diagram of the transducer at zero velocity of the normal ear: the can (a) and the magnet (b).

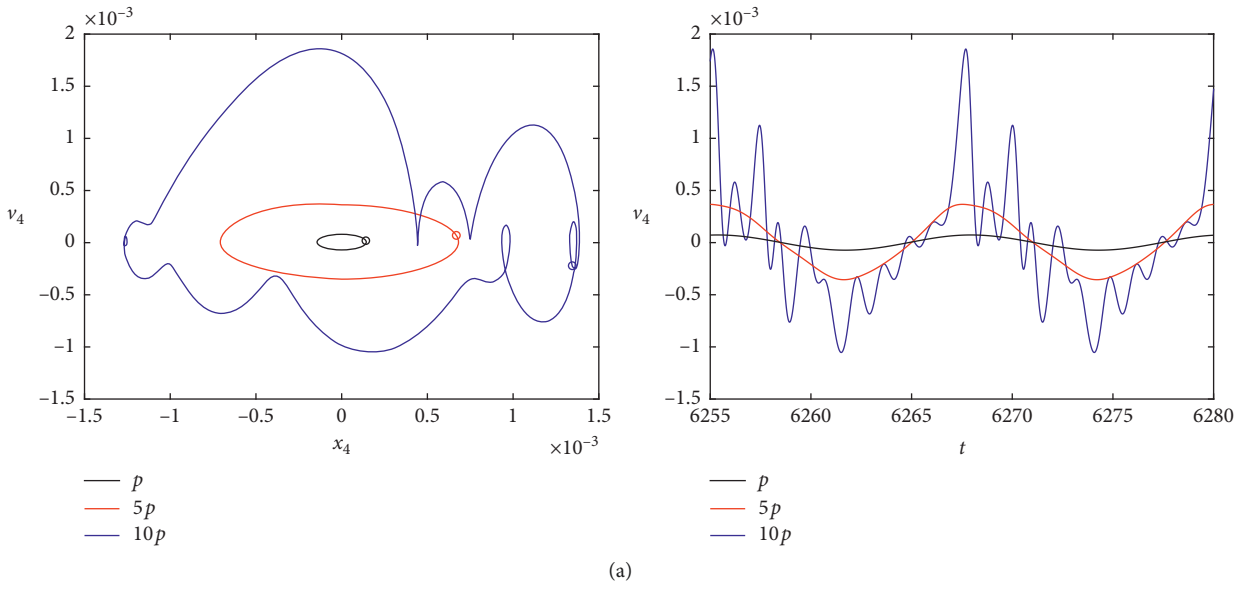

Figure 22: Continued.

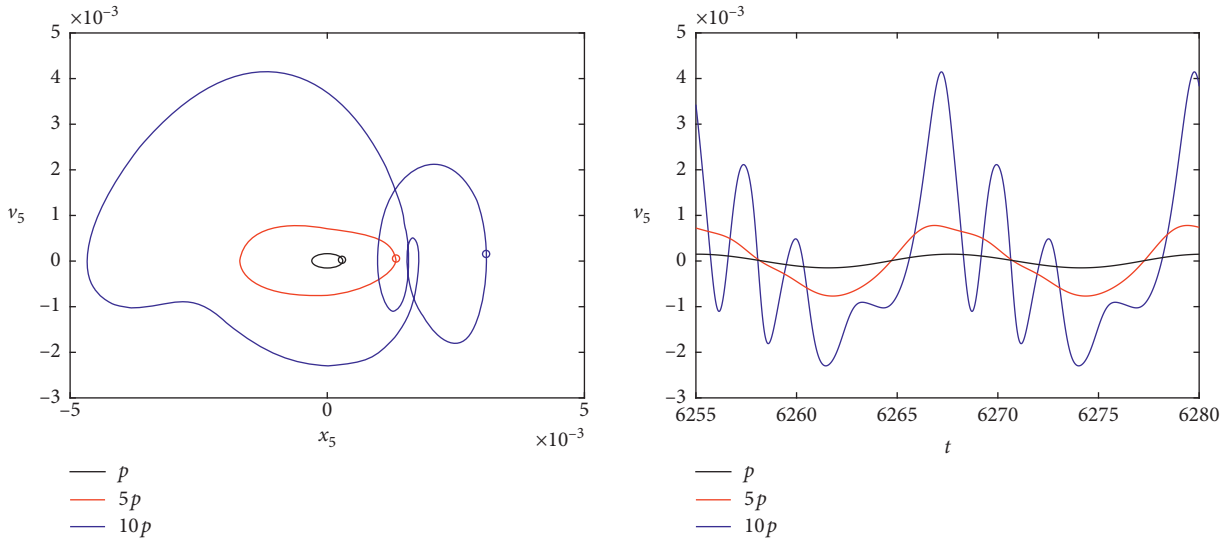

(b)

Figure 22: Phase diagram and time series of the transducer for the normal ear for Ω = 0.5: the can (a) and the magnet (b).

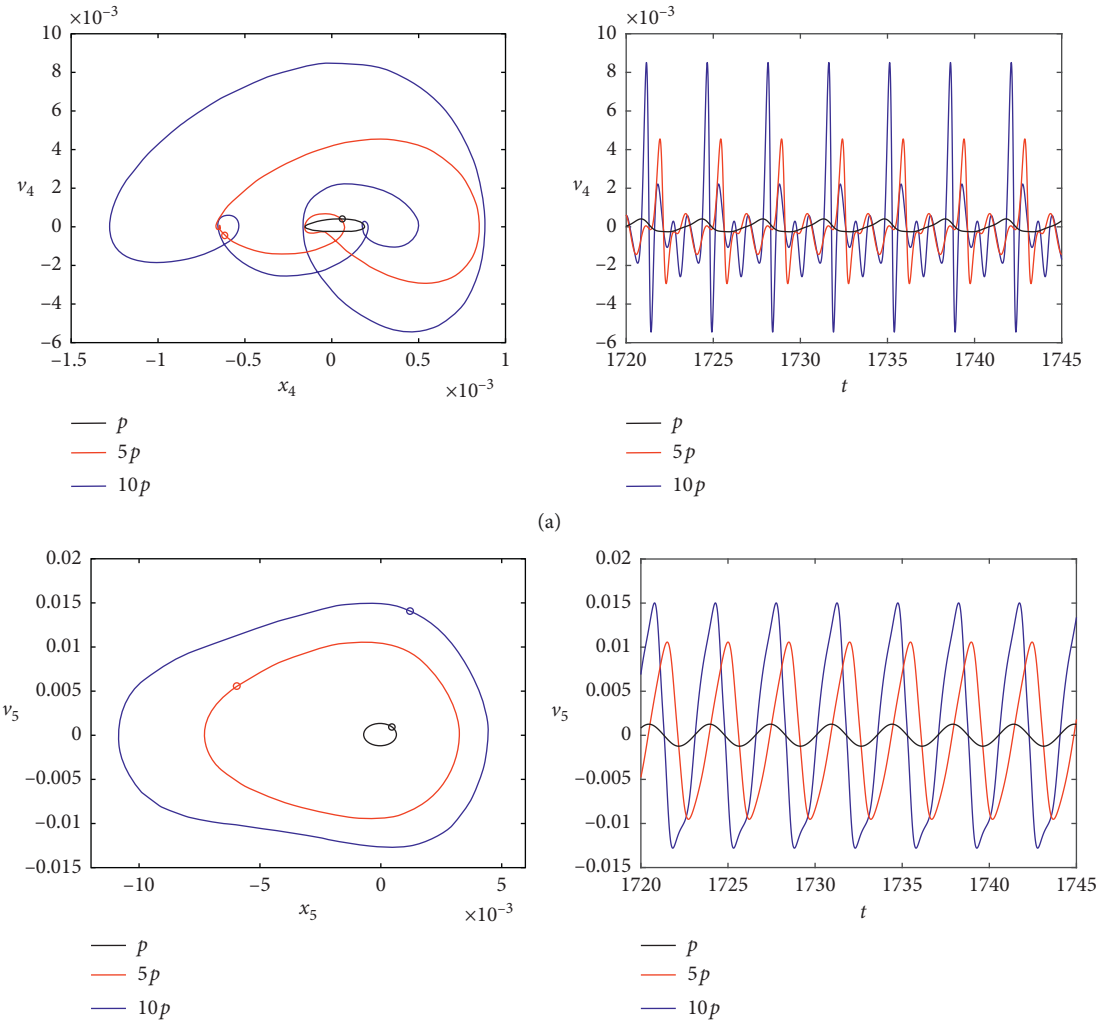

(a)

(b)

Figure 23: Phase diagram and time series of the transducer for the normal ear for Ω = 1.8: the can (a) and the magnet (b).

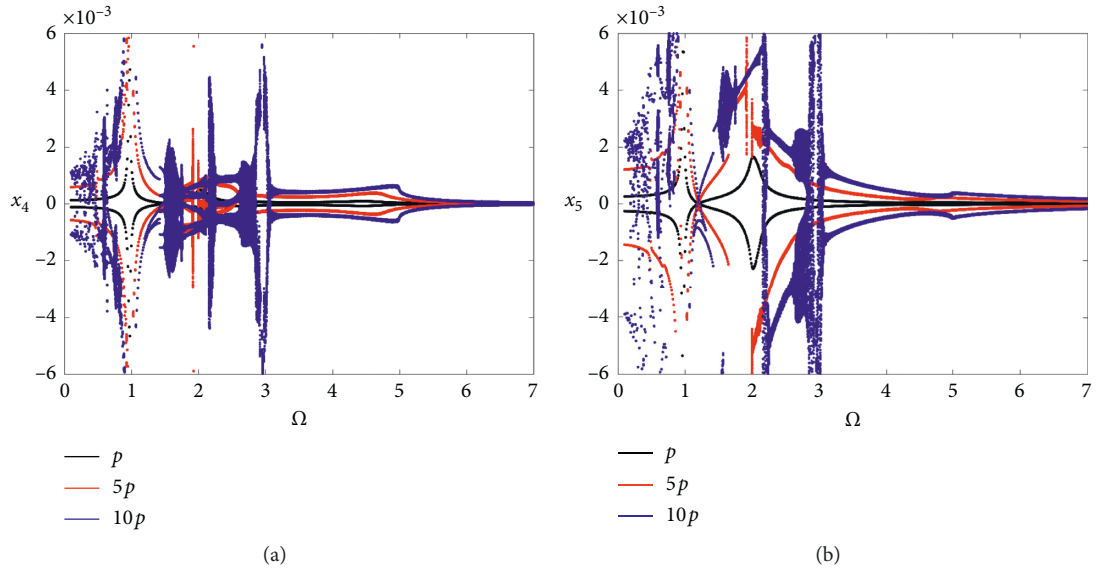

Figure 24: Bifurcation diagram of the transducer at zero velocity of the pathological ear: the can (a) and the magnet (b).

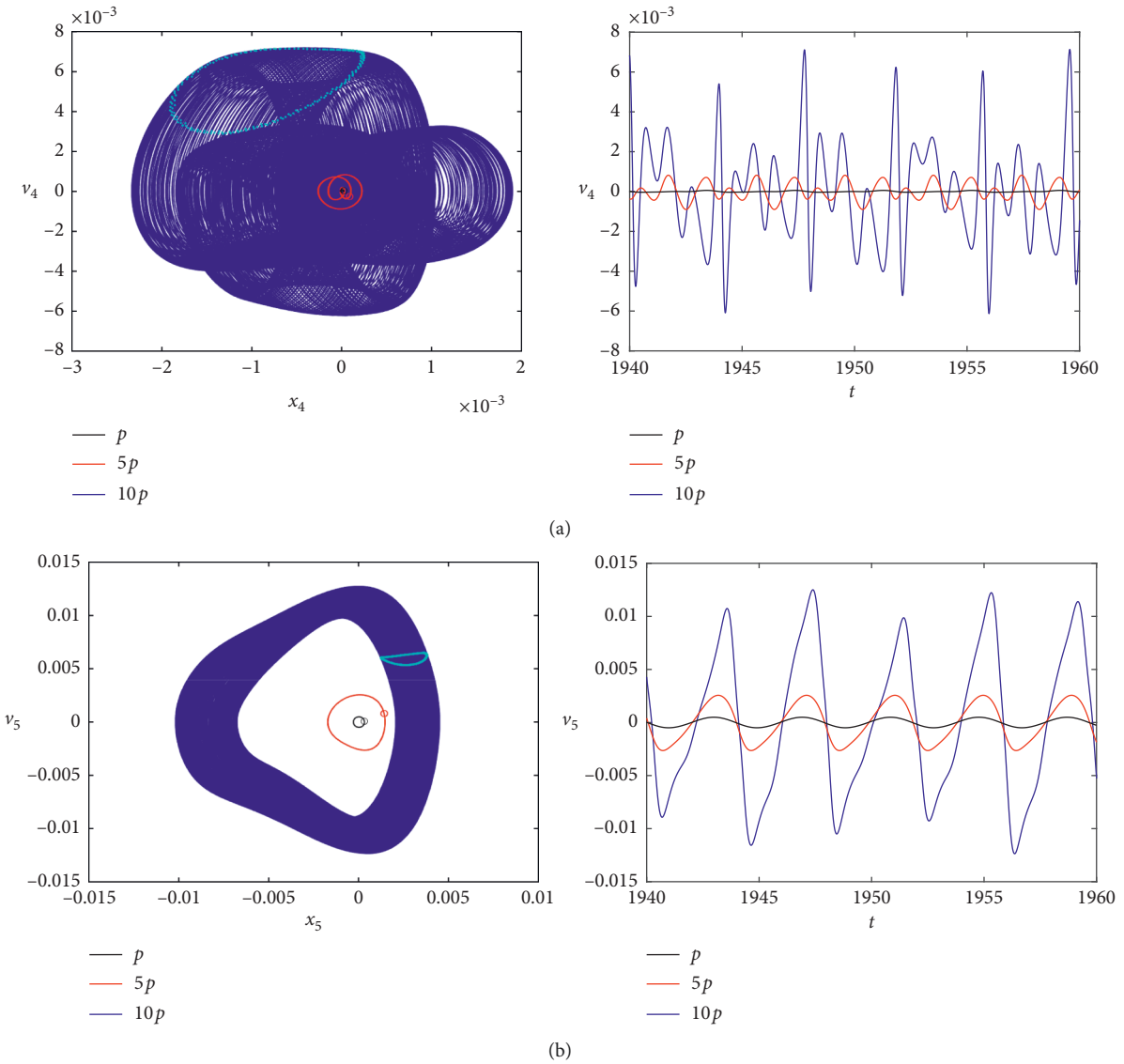

Figure 25: Phase diagram and time series of the transducer for the pathological ear for $\Omega = 1.6$: the can (a) and the magnet (b).

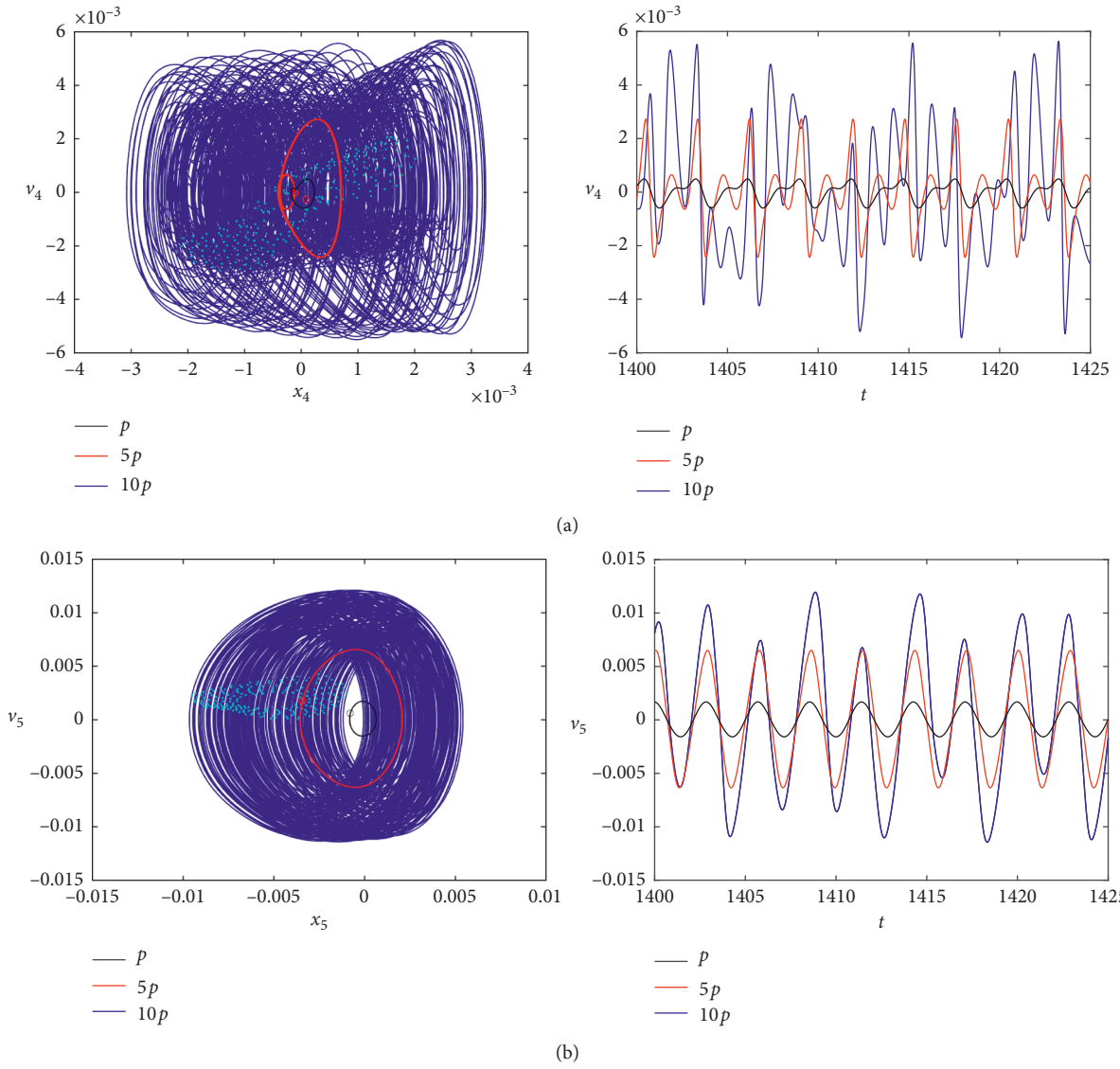

Figure 26: Phase diagram and time series of the transducer for the pathological ear for $\Omega = 2.2$: the can (a) and the magnet (b).

the same as excitation frequency (period 1 response). An increase in external excitation frequency to $\Omega = 1.8$ leads to regular vibrations without additional waves of the incus and the malleus, but the stapes still has an extra component even for excitation $5p$ and also $10p$ (see Figure 15). The situation is going on to $\Omega = 2.1$. For $\Omega > 2.1$, the stapes, the same as the incus and the malleus, vibrates harmonically.

Decrease in damping completely changes middle ear dynamics, although regular motion is still possible between $1 < \Omega < 2$ (Figure 12), providing that the excitation amplitude is not so high (e.g., p and $5p$). Stapes motion (Figure 12(c)) is more complicated than the malleus (Figure 12(a)) and the incus (Figure 12(b)) for strong excitation ($10p$). However, when $\Omega = 1.6$, all the ossicles vibrate quasi-periodically (Figure 16). Then, the Poincaré points create a shape like a circle. An increase in excitation frequency leads to another chaotic region mainly of the stapes, e.g., for $\Omega = 2.2$ (Figure 17(c)). Fortunately, chaos is observed only for strong enough excitation ($10p$, blue colour), and it disappears for $\Omega > 3.0$. This observation is proved by the Lyapunov maximal exponent (Figure 18). Positive values of the exponent exhibit a chaotic region in the IME system. A typical stimulation of the human middle ear during a normal life is between 60 dB and 100 dB. Dimensional external excitation of $P = 0.12$ mN corresponds to 50 dB, whereas dimensionless $10p$ means about 65 dB. Therefore, in most real situation, stimuli of the human ear should not exceed the value of p. Then, stapes motion is regular, sometimes with another harmonic component (polyharmonics) but still regular.

In the next section, a question of the FMT behaviour fixed to the incus for the help of the clip is analysed as well.

4.3. Dynamics of the transducer. The transducer is an extra element in the middle-ear structure which stimulates ear

dynamics but on the contrary, the transducer is stimulated by the incus. Qualitative analysis of motion of the can (x_4) and the magnet (x_5) of the transducer is shown in Figures 19 and 20 for standard and pathological ear parameters, appropriately. Still, the gray regions represent irregular motion while the white ones irregular behaviour. In the case of the standard set of ear parameters (Figure 19), three variants of excitation (p, $5p$, and $10p$) cause only regular motion but with polyharmonic components between $0.5 < \Omega < 2$ visible on the bifurcation diagram (Figure 21) when excitation is $5p$ and $10p$. Motion of the can is characterized by a bigger number of harmonic components than that of the magnet. However, despite the fact that the magnet is forced harmonically, its response for $\Omega = 0.5$ is not harmonic but polyharmonic (Figure 22(b)). At that time, the can moves in the same manner (Figure 22(a)). For bigger excitation frequency ($\Omega = 1.8$), the can moves still polyharmonically (for p and $10p$, Figure 23(a)) but the magnet oscillates harmonically (Figure 22(b)). Behaviour of the can directly influences the incus motion; therefore, it explains the polyharmonic nature of the incus and the malleus in the IME. The situation changes when damping coefficients are small (the pathological ear, Figure 20). Then, excitation greater (or equal) than $5p$ causes chaotic behaviour of the can (Figure 20(a)) and the magnet as well (Figure 20(b)). The gray region of chaotic motion exists for all the range of frequencies (Ω) contrary to the standard ear parameters (Figure 19) where chaotic motion disappears completely for $\Omega > 7$. Bifurcation diagrams (Figure 24) show that irregular motion of the can (Figure 24(b)) and the magnet (Figure 24(b)) exists for different values of Ω. For example, when $\Omega = 1.6$, motion of the can and the magnet is regular and harmonic for excitation equals p (Figure 25). When excitation increases to $5p$, polyharmonic motion of the can (Figure 25(a)) corresponds to harmonic motion of the magnet (Figure 25(b)), whereas for strong excitation ($10p$), the can and the magnet vibrate polyharmonically and quasi-periodically. A more difficult situation is observed for $\Omega = 2.2$ (Figure 26), where chaotic (blue) attractor appears for strong excitation.

5. Discussion and Conclusions

The normal human middle ear, analysed on the basis of the 3dof model, is fully predictable in the real range of excitation. Periodic excitation of the malleus is transferred to the stapes also as a periodic signal. Even for decreased system damping (pathological ear), the regular stimulation gives the regular output. However, introducing the transducer to the middle ear structure changes ear dynamics. It is important for the implemented ear to have the same or very close characteristics to the normal, healthy ear. Therefore, the transducer should be small enough and low weight.

The implanted human middle ear is also fully predictable in the real range of excitation and standard parameters. At low excitation frequencies, ossicular chain motion in the implanted ear is still regular, but not always harmonic. For stronger excitation, another harmonic component appears in the system response. This effect is probably caused by nonlinearities and internal resonances in the multi-degree-of-freedom system. However, real danger can appear when damping of the system is decreased. Then, even chaotic vibrations can be generated for strong excitation.

The floating mass transducer presented here works correctly in low-frequency range. Where the frequency is higher than about 5 kHz, the amplitude of stapes motion drastically falls down because the motion of FMT, especially the can, decreases. Interestingly, the harmonic motion of the magnet is converted to polyharmonic can's motion which is next transferred to the ossicles. Unfortunately, the implant does not work correctly in case of the pathological ear, e.g., when damping properties are lower.

Polyharmonic motion of the stapes in the IME is the problem that should be solved in order to improve hearing quality. Polyharmonic effect is probably caused by internal resonances in the 5dof system. The question of additional harmonics and phase shift needs probably correctness of implant parameters. Stiffness of the silicon springs and the coupler is another important parameter of the IMEHD that should be analysed with special care in the future.

Data Availability

The numerical data used to support the findings of this study are available from the corresponding author upon request.

Conflicts of Interest

The authors declare that they have no conflicts of interest.

Acknowledgments

This research was financed in the framework of the project "Nonlinear effects in middle ear with active implant," no. 2018/29T8/01293, funded by the National Science Centre, Poland.

References

[1] H. Liu, D. Xu, J. Yang, S. Yang, G. Cheng, and X. Huang, "Analysis of the influence of the transducer and its coupling layer on round window stimulation," *Acta of Bioengineering and Biomechanics*, vol. 19, no. 2, pp. 103–111, 2017.

[2] E.-P. Hong, M.-K. Kim, I.-Y. Park, S.-H. Lee, Y. Roh, and J.-H. Cho, "Vibration modeling and design of piezoelectric floating mass transducer for implantable middle ear hearing devices," *IEICE Transactions on Fundamentals of Electronics, Communications and Computer Sciences*, vol. E90–A, no. 8, pp. 1620–1627, 2007.

[3] R. M. Lord, R. P. Mills, and E. W. Abel, "An anatomically shaped incus prosthesis for reconstruction of the ossicular chain," *Hearing Research*, vol. 145, no. 1-2, pp. 141–148, 2000.

[4] D. P. Morris, M. Bance, and R. G. van Wijhe, "How do cartilage and other material overlay over a prosthesis affect its vibration transmission properties in ossiculoplasty?," *Otolaryngology-Head and Neck Surgery*, vol. 131, no. 4, pp. 423–428, 2004.

[5] K. R. Williams and T. H. J. Lesser, "A finite element analysis of the natural frequencies of vibration of the human tympanic

membrane. part i," *British Journal of Audiology*, vol. 24, no. 5, pp. 319–327, 1990.

[6] K.-W. Seong, E.-S. Jung, H.-G. Lim, and J.-W. Lee, "Vibration analysis of human middle ear with differential floating mass transducer using electrical model," *IEICE Transactions on Information and Systems*, vol. E92-D, no. 10, pp. 2156–2158, 2009.

[7] M. E. Ravicz, J. J. Rosowski, and S. N. Merchant, "Mechanisms of hearing loss resulting from middle-ear fluid," *Hearing Research*, vol. 195, no. 1-2, pp. 103–130, 2004.

[8] H. H. Nakajima, M. E. Ravicz, S. N. Merchant, W. T. Peake, and J. J. Rosowski, "Experimental ossicular fixations and the middle ear's response to sound: evidence for a flexible ossicular chain," *Hearing Research*, vol. 204, no. 1-2, pp. 60–77, 2005.

[9] B. Feng and R. Z. Gan, "A lumped-parameter mechanical model of human ear for sound transmission," in *Proceedings of the Second Joint 24th Annual Conference and the Annual Fall Meeting of the Biomedical Engineering Society] [Engineering in Medicine and Biology*, vol. 1–3, pp. 267-268, Houston, TX, USA, October 2002.

[10] M. Lauxmann, A. Eiber, F. Haag, and S. Ihrle, "Nonlinear stiffness characteristics of the annular ligament," *The Journal of the Acoustical Society of America*, vol. 136, no. 4, pp. 1756–1767, 2014.

[11] B. Darvish, S. Najarian, E. Shirzad, and R. Khodambash, "A novel tactile force probe for tissue stiffness classification," *American Journal of Applied Sciences*, vol. 6, no. 3, pp. 512–517, 2009.

[12] Y. Zhang, B. Tang, and X. Xiao, "Time-frequency interpretation of multi-frequency signal from rotating machinery using an improved Hilbert-Huang transform," *Measurement*, vol. 82, pp. 221–239, 2016.

[13] R. Rusinek, M. Szymanski, J. Warminski, M. Zadrozniak, and K. Morshed, "Vibrations in the human middle ear," *Medical Science Monitor*, vol. 17, no. 12, pp. BR372–BR376, 2011.

[14] R. Rusinek, J. Warminski, M. Szymanski, K. Kecik, and K. Kozik, "Dynamics of the middle ear ossicles with an sma prosthesis," *International Journal of Mechanical Sciences*, vol. 127, pp. 163–175, 2017.

[15] M. Szymanski, R. Rusinek, M. Zadrozniak, K. Morshed, and J. Warminski, "The influence of incudostapedial joint separation on the middle ear transfer function," *Clinical and Experimental Otorhinolaryngology*, vol. 7, no. 4, pp. 250–253, 2014.

[16] R. Rusinek, J. Warminski, M. Zadrozniak, and M. Szymanski, "Nonlinear approach to modelling of otosclerosis in a human middle ear," *Differential Equations and Dynamical Systems*, vol. 21, no. 1-2, pp. 45–57, 2013.

[17] R. Rusinek, J. Warminski, A. Weremczuk, and M. Szymanski, "Analytical solutions of a nonlinear two degrees of freedom model of a human middle ear with sma prosthesis," *International Journal of Non-linear Mechanics*, vol. 98, pp. 163–172, 2018.

[18] D. P. Morris, M. Bance, R. G. van Wijhe, M. Kiefte, and R. Smith, "Optimum tension for partial ossicular replacement prosthesis reconstruction in the human middle ear," *The Laryngoscope*, vol. 114, no. 2, pp. 305–308, 2004.

[19] S. E. Voss, J. J. Rosowski, S. N. Merchant, and W. T. Peake, "Acoustic responses of the human middle ear," *Hearing Research*, vol. 150, no. 1-2, pp. 43–69, 2000.